A Fieldable Process for Sensitive Detection of Airborne Viruses via Electrophoresis-based RNA Enrichment

Huifeng Du[1,†], Simone Bruno[1,†], Kalon J. Overholt[2,†], Sebastian Palacios[1, 2,†], Hsin-Ho Huang[1], Carlos Barajas[1], Ben Gross[1], Cindy Lee[1], Haley K. Evile[2], Nuno Rufino de Sousa[3], Antonio Gigliotti Rothfuchs[3], and Domitilla Del Vecchio[1,*]

[1] *Department of Mechanical Engineering, Massachusetts Institute of Technology, 77 Massachusetts Avenue, Cambridge, MA 02139.*

[2] *Department of Biological Engineering, Massachusetts Institute of Technology, 77 Massachusetts Avenue, Cambridge, MA 02139.*

[3] *Department of Microbiology, Tumor and Cell Biology (MTC), Karolinska Institutet, Stockholm, Sweden.*

[†] *These authors contributed equally: H. Du, S. Bruno, K.J. Overholt, and S. Palacios*

[*] *Corresponding Author: Email:* ddv@mit.edu

Abstract: Sensitive, on-site, virus detection is a requirement for timely action against the spread of airborne infection since ultra-low in-air viral concentrations can readily infect individuals when inhaled. Here, we consider a fieldable biosensing process that incorporates a fast RNA enrichment step in order to concentrate viral RNA in a small volume prior to RT-qPCR. The enrichment approach uses electrophoresis in an RT-qPCR-compatible buffer, and allows to concentrate the RNA by nearly 5-fold within only 10 minutes. In order to place this performance into context, we analyzed the minimum detectable concentration of a low-cost, fieldable, biosensing process that uses electrostatic precipitation for air sampling, heating for viral RNA extraction, and then RNA enrichment, followed by RT-qPCR. With enrichment, we estimated an in-air concentration of 5654 genome copies (gc)/m^3 with a 100% detection rate and an in-air concentration of 4221 gc/m^3 with a 78.6% detection rate. Given that the concentrations of common viruses, such as influenza and SARS-CoV-2, in several indoor spaces are between 5800 and 37000 gc/m^3, we conclude that enrichment allows a detection that is sufficiently sensitive for practical applications.

Keywords: Airborne Viruses; RNA Enrichment; RT-qPCR ;Biosensors; Virus Detection; Electrophoresis

1 Introduction

The COVID-19 pandemic has demonstrated how vulnerable we are to the spread of airborne infectious diseases. It is also not an isolated case, but rather it follows a series of other epidemics, although not as devastating, including SARS (2003), Swine Flu (2009), MERS (2012), Ebola (2014), and the 2018 United States adenovirus outbreak [1, 2, 3, 4, 5, 6]. With a major epidemic every 2-6 years, we are at continuous risk for the spread of novel infectious diseases. At the same time, even common viruses, such as influenza, respiratory syncytial virus (RSV), and now also SARS-CoV-2, have major repercussions every year among vulnerable populations, leaving behind deaths and healthcare expenses [7, 8, 9, 10].

Early detection is required for timely action and acting quickly has been proven one of the most effective means to contain an epidemic [11, 12, 13]. Currently, despite the numerous COVID-19, influenza and RSV surveillance programs [14, 15, 16], there is an average delay of nearly 6 days between the onset of symptoms and diagnosis [17, 18]. Conventional detection methods depend on symptom-based viral testing, with an average viral shedding duration of 16 days observed among presymptomatic individuals [19, 20]. Environmental monitoring approaches that sample the air of indoor spaces and rapidly analyze it for the presence of pathogens are more practical approaches that could reduce costs, improve detection speed, and minimize disruption to schedules.

Currently, there are no established processes for rapid detection of pathogens in indoor air. Common approaches include sampling the air with a pump and then processing the sample in a laboratory, which takes

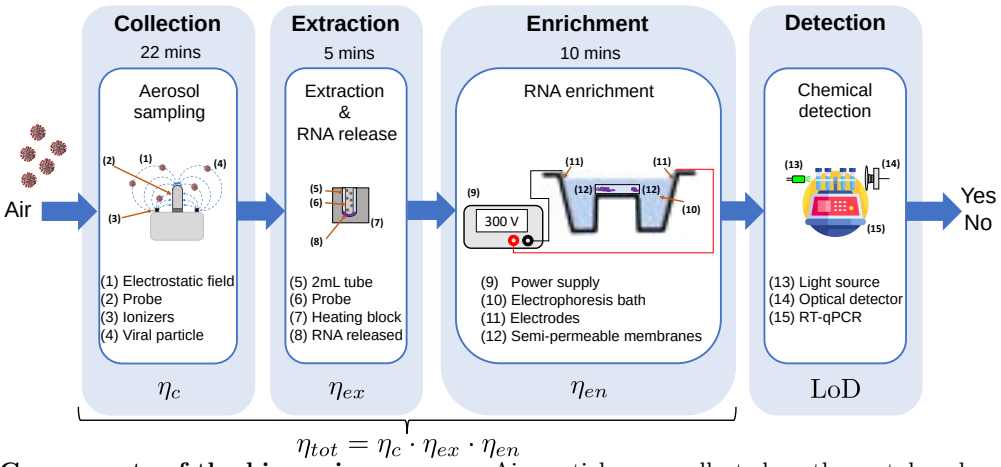

Figure 1: **Components of the biosensing process.** Air particles are collected on the metal probe of an aerosol sampler, which uses electrostatic precipitation (ESP) and follows the design of [26]. After sampling for 22 minutes, the metal probe with collected particles is placed in a 2 mL tube with 220 µL of nuclease-free water and goes through heating at 98 °C for 5 minutes. The water with the sample is then entirely transferred to an enrichment device, which performs electrophoresis against a semipermeable membrane for 10 minutes. Upon completion, the 7.4 µL of sample next to the membrane is drawn and taken to chemical detection. This employs RT-qPCR with primers specific to the viral target. Each step performance is characterized in terms of its efficiency η. The variables η_c, η_{ex}, and η_{en} are the efficiencies of the collection, extraction, and enrichment steps, respectively, as defined in Section "Process efficiencies" of Supplementary Materials. LoD is the limit of detection of RT-qPCR, and η_{tot} represents the efficiency of the overall process.

days (BioWatch program [21] and similar [22]). Technologies such as the Thermo Scientific's AerosolSense Sampler and Bertin Technologies' Coriolis µ, with their separate PCR processes, can be used to detect common respiratory pathogens, including SARS-CoV-2, Flu A/B and/or RSV, and microbes on-site [23, 24, 10, 25]. However, the air samplers are expensive, the times of collection and analysis required to hit useful detectable concentration remain long, and the whole process requires technical expertise to run and interpret. These approaches are thus largely incompatible with rapid detection and with adoption in lower-resource locations where surveillance and containment are needed.

In this work, we thus consider a biosensing process that uses electrostatic precipitation (ESP) for air sampling and heating for extraction of RNA from viral particles (Figure 1). ESP is an alternative low-cost air sampling technology, which has proven effective for detection of microbes and active viruses such as SARS-CoV-2 in indoor spaces [26, 27, 28, 29]. Because collection occurs on a metal probe, a relatively small volume of water is required to cover the probe's surface and extract the viral genetic material through heating [26] (Figure 1, Collection and Extraction). In turn, extraction of genetic material from viruses using heat has already found use in fieldable diagnostic tests, given its simplicity and low cost [30, 31]. Between extraction and detection, we introduce an RNA enrichment step, which concentrates the genetic material in a small volume using electrophoresis in a custom-made RT-qPCR compatible buffer. We theoretically and experimentally characterize the enrichment performance and then put this performance into the context of the biosensing process. To this end, we measure experimentally the efficiency of each step in isolation, and then the combined detection rate of the steps downstream of collection by directly loading known amounts of inactivated SARS-CoV-2 virus on the ESP sampler's metal probe. Finally, we translate this combined detection rate to in-air particle concentration that we can detect based on the collection efficiency of the ESP sampler.

2 Results

The biosensing process is depicted in Figure 1. In this process, air sampling through ESP collects aerosols on a metal probe, which is then taken to a tube filled with water for heat-based extraction of the viral RNA. The water with the extracted RNA is then transferred to the enrichment device channel. The enriched sample is

then taken to the RT-qPCR tube for chemical detection. We evaluate the performance of the whole process by its minimum detectable concentration (MDC) C_{min}, that is, the lowest concentration of viral particles in the air (in genome copies per m^3 of air) that can be detected with a detection rate of at least 95%. To this end, we define the efficiency of the whole process η_{tot} as the ratio between the number of genome copies resulting in the 20 µL RT-qPCR reaction volume and the number of corresponding viral genome copies per m^3 of air. With η_{tot} defined this way, and with LoD being the limit of detection of RT-qPCR (expressed in copies / µL), the minimum detectable concentration of the process is given by

$$C_{min} = \frac{\text{LoD} \cdot V_{\text{PCR}}}{\eta_{tot}}, \tag{1}$$

where $V_{\text{PCR}} = 20\,\mu\text{L}$ is the final RT-qPCR reaction volume. We first estimate C_{min} by experimentally characterizing the efficiency of each step of the process in isolation, and by then calculating η_{tot} as the product of the efficiencies of each step. Letting $\eta_c, \eta_{ex}, \eta_{en}$ represent the efficiency of the collection, extraction and enrichment step, respectively (see "Process efficiencies" of Supplementary Materials for definitions), the overall process efficiency, η_{tot}, is given by

$$\eta_{tot} := \eta_c \cdot \eta_{ex} \cdot \eta_{en}. \tag{2}$$

In Section 2.1, we characterize the efficiency of the ESP air sampler η_c. This allows us to obtain a mapping between the number of particles collected on the metal probe and the particle concentration in air. In Section 2.2, we quantify the efficiency of the extraction step, η_{ex}, while in Section 2.3, we quantify the efficiency of the enrichment step η_{en}. In order to also account for the potential losses associated with the transfer of material between the steps, we perform an integration test in Section 2.4. In this test, we directly load known copies of inactivated SARS-CoV-2 virus on the metal probe of the sampler and perform heat extraction, enrichment, RT-qPCR, and evaluate detection rate. Finally, in Section 2.5, we translate the copy numbers on the metal probe to in-air concentration of viral particles that we can detect using the collection efficiency of the ESP air sampler. The overall process performance is also estimated in Section 2.5.

2.1 Characterization of collection efficiency

In order to obtain a mapping between the number of particles collected on the metal probe and the in-air particle concentration, we performed experiments in a containment tent where we nebulized fluorescent beads in known quantity (Figure 2(a)-(c)) and then measured the amount of collected beads on the metal probe via flow cytometry. The ESP sampler used in this study is the same as employed to recover active SARS-CoV-2 [27] and viable *Bacillus atrophaeus* [26] from air, demonstrating its efficacy in capturing a range of airborne pathogens. Although the SARS-CoV-2 virus is approximately 100 nm in diameter, the aerosols that transport these viruses exhibit different size distributions [32]. It is also known that the aerosol size determines the airborne transmission and detection efficiency in environmental monitoring [33]. Specifically, research indicates that smaller aerosol particles less than 5 µm in size contain the majority of airborne viruses [34]. SARS-CoV-2 aerosols have been shown to be around 1 µm in diameter [35, 36], with viral RNA predominantly found in particles between 0.5 to 4 µm [33, 37]. We therefore selected 1 µm-size beads to emulate the most prevalent size of airborne virus particles. Furthermore, the Omron nebulizer (NEC801) that we used produces droplets primarily in the 1-10 µm range [38], thereby providing the desired droplet size.

The results of the collection experiments are shown in Figure 2(d). On the x-axis we report the *average bead concentration in the tent* over the sampling time interval T, that is $\bar{C} = \frac{1}{T}\int_0^T C(t)dt$, in which $C(t)$ represents the instantaneous concentration in the tent at time t and $T = 22$ min. On the y-axis we plot the number of collected beads with the collection efficiencies as calculated from the definition in Figure 2(a). The average bead concentrations that we used are consistent with the reported concentrations of influenza virus present during flu season in enclosed environments such as daycare centers and airplanes, ranging from 5,800 to 37,000 copies per m^3 [39]. Specifically, we chose four values of $\bar{C}$ that fall within the lower half of this range. The efficiency of collection is $\eta_c = 0.10 \pm 0.001$ at the lowest concentration of $4200\,\text{B/m}^3$ and $\eta_c = 0.083 \pm 0.005,\ 0.067 \pm 0.002,\ 0.10 \pm 0.002$ for concentrations $\bar{C} \approx 8300\,\text{B/m}^3,\ 12\,000\,\text{B/m}^3,\ 17\,500\,\text{B/m}^3$, respectively (Figure 2(d)).

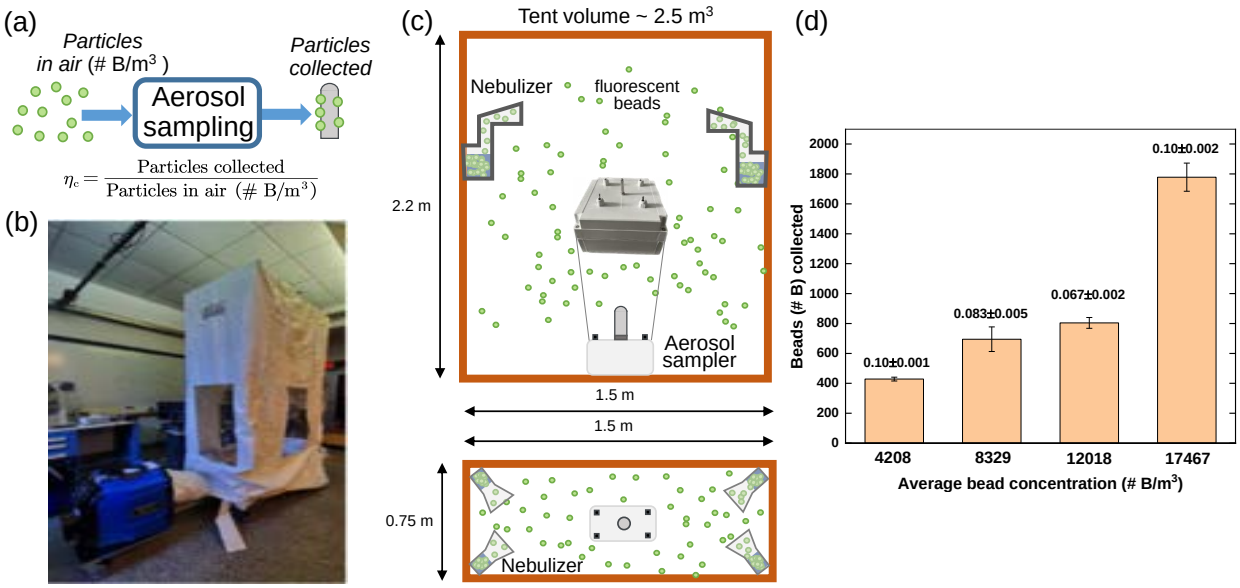

Figure 2: **Characterization of the collection efficiency through ESP.** (a) Schematic of the collection process and definition of the collection efficiency η_c. (b) Containment tent where beads were nebulized. (c) Experimental setup: the containment tent is 2.54 m^3 with the sampler at the center. At the top four corners we placed four nebulizers from which we nebulized fluorescent beads (B) into the tent. (d) Bar chart showing the number of beads ($\#B$) recovered from the metal probe of the ESP device at the end of $T = 22$ min of sampling. On the x-axis we indicated the average bead concentrations in the tent $\bar{C}$ ($\#B/m^3$) and on the y-axis the number of beads collected. The average and standard deviation was computed based on three experimental replicates using the definition in panel (a). The data was background-subtracted, that is, subtracting the amount of beads collected with only deionized water nebulized (see "Collection" in Supplementary Materials for details).

2.2 Characterization of heat extraction efficiency

In this section, we evaluated the efficiency of using heat for extracting genetic materials from viral particles attached on the metal probe of the ESP sampler (Figure 3(a)). Heat-based extraction, a method proven effective in other portable biosensing applications [40], facilitates the release of genetic material from viruses without necessitating extra chemicals. We tested two different numbers of genome copies in a 10 µL volume that we loaded on the metal probe: 2378 and 220000. The copy numbers were obtained from the maximum concentration tested on the RT-qPCR standard curves (see Figure 4(e) and "RT-qPCR" in Supplementary Materials), and from a concentration of 1000 copies / µL, respectively, when resuspended in 220 µL of solution. By comparing the Ct (cycle threshold) values against the standard curve of RT-qPCR at known concentrations of synthetic SARS-CoV-2 RNA in nuclease-free water (Figure 3(b)), we quantified the extraction efficiency following the definition in Figure 3(c). We conclude that the efficiencies are 0.115 ± 0.092 and 0.129 ± 0.086 (Figure 3(d)), for the number of copies loaded on the metal probe at 2378 and 220000, respectively (see Methods 4.3 and "Heat extraction" in Supplementary Materials for details).

The large standard deviation can be attributed to the composition of the input material, which includes proteins, lipid membranes and other cell lysates that may interfere with RT-qPCR, and the damage of the target during heat inactivation at the manufacturing facility. In fact, this material has been heat-inactivated at 65 °C for 30 minutes, so it is possible that the genetic material may have already been damaged to different degrees. High variability using this material for extraction of viral RNA was reported before [41], indicating the need for quantitative controls with higher integrity and purity for more accurate characterization of the virus extraction efficiency. Nevertheless, to demonstrate that the variation in data was not caused by our loading experimental protocol, we also loaded the metal probe with FluoSpheres and repeated the above procedure, excluding the heating treatment. We measured the number of recovered FluoSpheres using flow cytometry. The results reported in Figure S2 support that the variation in outcomes was due to the starting material and not to our protocol.

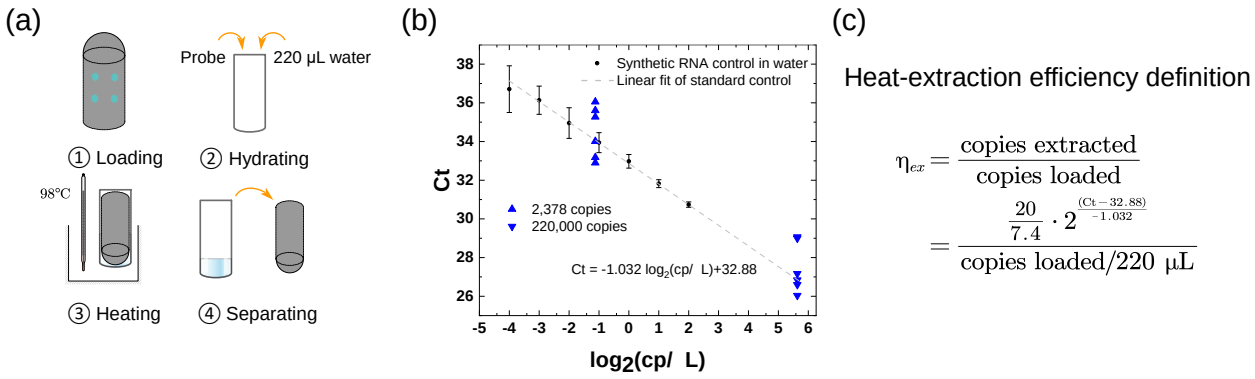

(d) Heat-extraction efficiency calculation

	1	2	3	4	5	6	Statistics
2,378 copies	0.117	0.040	0.205	0.050	0.247	0.030	0.115±0.092
220,000 copies	0.176	0.152	0.258	0.036	0.033	0.122	0.129±0.086

Figure 3: **Heat extraction efficiency characterization.** (a) A known number of genome copies of ATCC virus in a 10 µL volume are loaded on the metal probe in 1 µL droplets. The probe is then air-dried for 5 minutes before being collected into a 2 mL microcentrifuge tube. The tube is then heated at 98 °C for 5 minutes. The metal probe is removed after cooling down and the liquid is analyzed with RT-qPCR. (b) Ct values from RT-qPCR after heat extraction plotted as blue triangles on the standard curve for two different numbers of genome copies. For each copy number, N=6 biological replicates were obtained. See Tables S1 and S2 for complete data, including negative control (no-heating) and positive control (same number of copies in water). (c)-(d): The definition (c) and the calculation (d) of the heat-extraction efficiencies at two different genome copies.

2.3 Development and characterization of nucleic acid enrichment in solution

We built a custom system to enrich the concentration of nucleic acid in solution with the ultimate goal of lowering the minimum detectable concentration of the overall biosensing process. The working principle of the enrichment module is as follows. Negatively charged nucleic acid migrates via electrophoresis in the opposite direction of an applied electric field (toward a positive electrode), but can be blocked by a semipermeable membrane allowing for ion exchange but not escape of large biomolecules, thereby causing nucleic acid to build up at high concentration against the membrane (Figure 4(a)). The enrichment device consists of a polydimethylsiloxane (PDMS) chip with a circular channel passing completely through the longest dimension of the chip. The channel was designed to accommodate exactly 250 µL of fluid, comparable to the volume of water in which the ESP sampler's metal probe is immersed for heat extraction (Figure 1). Both ends of the channel were sealed by semipermeable membranes bonded to the ends of the channels using PDMS (Figure 4(b)).

To perform enrichment, we first determined which conductive medium containing an analyte to be concentrated could be used to fill the channel. We tested the following buffers, including "ultra-fast" electrophoresis buffers: sodium boric acid (10 mM, pH 8), lithium boric acid (1 mM, pH 8.2), lithium acetate (5 mM) [42], and Tris-acetate (40 mM Tris, pH 8.3). Among them, lithium acetate (LA) demonstrated both desirably low thermal convection due to minimal Joule heating and a fast running speed. Therefore, we selected the LA buffer as the conductive medium in electrophoresis. After loading the channel with LA buffer containing an analyte, the enrichment module was placed in a standard electrophoresis bath containing LA buffer at 5 mM and a 300 V potential was applied between the electrodes, generating an electric field of approximately 2,000 V/m for a defined duration. See "Methods: RNA enrichment and quantification " and "Fabrication of enrichment devices" in Supplementary Materials for the fabrication and enrichment procedures.

To demonstrate the feasibility of the enrichment process, the device was first tested by loading 1 µg of mammalian RNA obtained from HCT 116 cells and stained with SYBR Green II. The imaging results are shown in Figure 4(c), which demonstrates an evolution from a uniform RNA concentration at 0 minutes

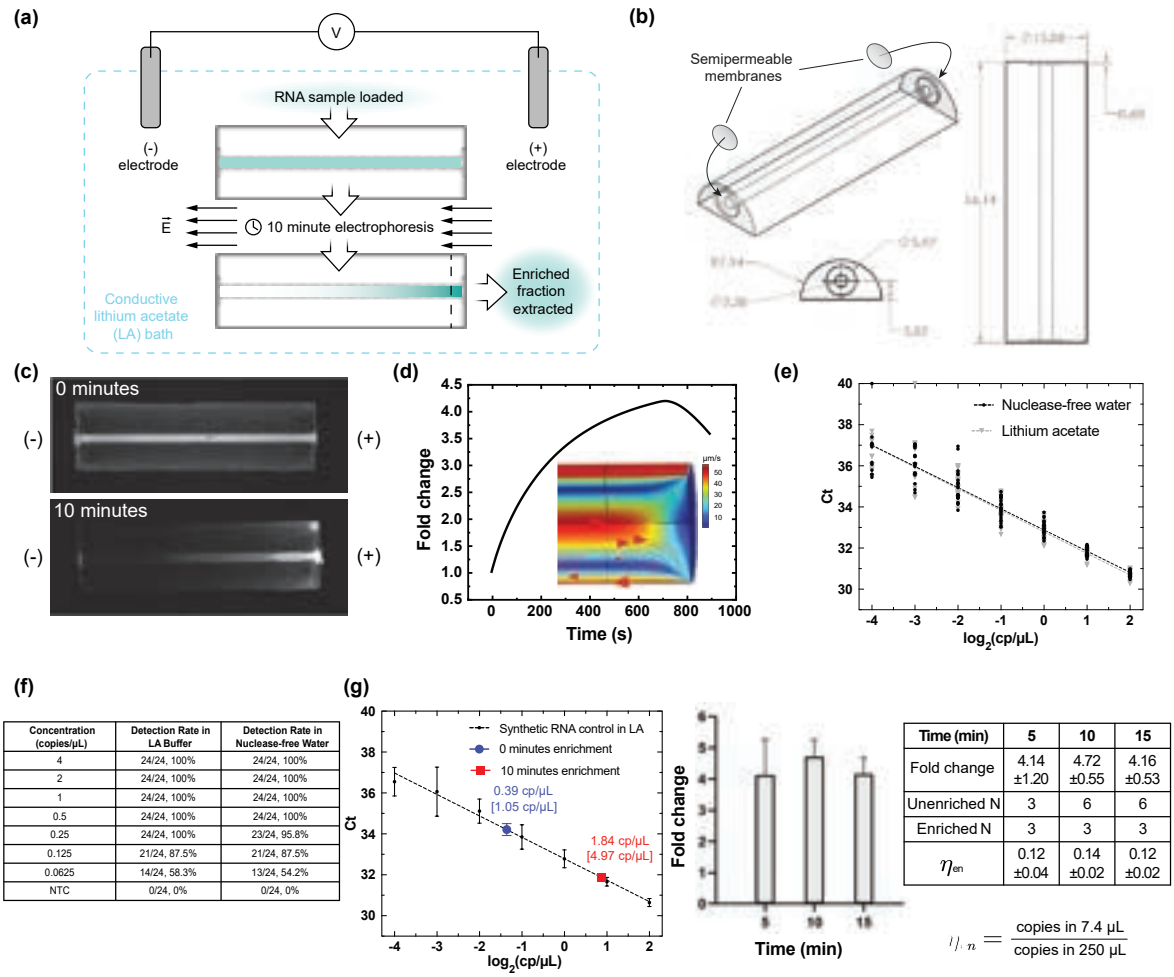

Concentration (copies/μL)	Detection Rate in LA Buffer	Detection Rate in Nuclease-free Water
4	24/24, 100%	24/24, 100%
2	24/24, 100%	24/24, 100%
1	24/24, 100%	24/24, 100%
0.5	24/24, 100%	24/24, 100%
0.25	24/24, 100%	23/24, 95.8%
0.125	21/24, 87.5%	21/24, 87.5%
0.0625	14/24, 58.3%	13/24, 54.2%
NTC	0/24, 0%	0/24, 0%

Time (min)	5	10	15
Fold change	4.14 ±1.20	4.72 ±0.55	4.16 ±0.53
Unenriched N	3	6	6
Enriched N	3	3	3
η_{en}	0.12 ±0.04	0.14 ±0.02	0.12 ±0.02

$$\eta_{en} = \frac{\text{copies in 7.4 μL}}{\text{copies in 250 μL}}$$

Figure 4: **Enrichment of RNA concentration at femtogram to microgram scales through membrane-coupled electrophoresis.** (a) Working principle of RNA enrichment. A 250 μL RNA sample buffered in 5 mM lithium acetate (LA) is loaded into a PDMS device consisting of a channel capped at both ends by semipermeable membranes. The device is immersed in an electrophoresis bath containing 5 mM LA and an applied voltage causes electrophoresis of RNA (teal) toward the positive terminal, concentrating the RNA against one of the membranes. An enriched fraction of RNA is then extracted adjacent to the membrane. (b) PDMS channel design for fast enrichment of nucleic acid. (Left) 3D view showing the location of semipermeable membranes in insets. (Center) Face-on view of channel and insets. (Right) Top view, rotated 90 degrees from that shown in (a). Dimensions are indicated in mm. (c) Images of microgram-scale enrichment of mammalian RNA stained with SYBR Green II in devices oriented as in (a), showing concentration profiles before enrichment (0 minutes) and after enrichment (10 minutes) at 2,000 V/m. Both images were obtained using identical exposure settings. (d) Multiphysics simulation of negatively charged particle migration in the enrichment device using COMSOL. Simulated time course of concentration fold change adjacent to the membrane (∼3% of device volume). Inset: simulated velocity streamlines. For details on the simulations, see "Supplementary Materials: Simulation of nucleic acid enrichment in enrichment devices." (e) Standard curves of RT-qPCR in nuclease-free water and LA buffer. We performed N=24 replicates for each condition across seven concentrations using synthetic SARS-CoV-2 RNA. (f) The detection rates at different concentrations for both LA buffer and nuclease-free water. The LoDs (limits-of-detection) were determined to be 0.25 copies / μL for both cases. Final concentration of LA buffer in RT-qPCR reaction is 1.85 mM. (g) Femtogram-scale enrichment of ultra-low concentration synthetic SARS-CoV-2 RNA. (Left) 10 minutes of enrichment leads to a 4.7-fold enrichment of RNA. Concentrations before and after enrichment are shown on the RT-qPCR standard curve in blue and red respectively, with bracketed and unbracketed values representing the concentrations in the device and RT-qPCR reactions, respectively. (Center) Fold change enrichment of synthetic SARS-CoV-2 RNA quantified by RT-qPCR at 5, 10, and 15 minutes. (Right) Summary of data collected, including enrichment efficiency η_{en}.

to a significant concentration gradient along the channel with enrichment at the positive terminal after only 10 minutes. We noted that the solution concentrates most strongly in the region directly adjacent to the membrane, suggesting that only a small extraction volume is needed to recover a highly concentrated RNA sample. The device was also tested using SYBR Safe™ Stain to visualize DNA (Thermo Scientific™, GeneRuler 1kb DNA Ladder, SM0312) migration over time (Figure S3). Together, these results confirmed that both DNA and RNA molecules can move toward and concentrate at the membrane adjacent to the positive terminal.

To estimate the expected fold change in RNA concentration, we performed a multiphysics simulation of the device using COMSOL (Figure 4(d)). This simulation incorporated electrokinetics and convective fluid flow (refer to "Simulation of nucleic acid enrichment in enrichment devices" in Supplementary Materials for simulation details), indicating that the concentration profile adjacent to the membrane is dictated by competing electrophoretic and electroosmotic effects. Electroosmotic flows dominate at longer time scales, causing the concentration of particles near the membrane to reach a maximum and eventually decrease. The simulated maximum degree of enrichment appeared to occur between 10 and 13 minutes.

To evaluate the impact of the LA buffer on RT-qPCR, we compared the standard curves and detection rates of RT-qPCR at known concentrations of synthetic SARS-CoV-2 RNA in LA buffer against those obtained in nuclease-free water. For the standard curves (Figure 4(e)), we conducted linear regression analysis to establish the relationship between the target's concentration in the RT-qPCR reaction and the Ct values. The LoD of RT-qPCR was defined as the lowest concentration of SARS-CoV-2 (copies / µL) at which the detection rate was 95% or higher. For both samples diluted in nuclease-free water or LA buffer, the LoD obtained was 0.25 copies / µL. NTCs in either nuclease-free water or LA buffer showed no detection (Figure 4(f) and S4). We concluded that LA buffer did not affect the RT-qPCR standard curve for detecting SARS-CoV-2 RNA.

To experimentally explore the required running time and estimate the concentration fold-change after the enrichment, we performed enrichment on ultra-low concentration of synthetic SARS-CoV-2 RNA at 5, 10 and 15 minutes, which lie around the optimum predicted by the simulations (Figure 4(d)). We chose the copy number of SARS-CoV-2 RNA at 0.39 copies / µL in the 20 µL RT-qPCR reaction volume (1.05 copies / µL in the electrophoresis channel), in order to achieve a pre-enrichment concentration close to the LoD of RT-qPCR (0.25 copies / µL, Figure 4(f)). The total mass of RNA loaded in the device was less than 4 femtograms (See "Enrichment" in Supplementary Materials for how this number was calculated). The Ct values obtained before and after enrichment were used to calculate the fold change in RNA concentration (Table S3). We found that the maximal fold change was approximately 5-fold after 10 minutes of enrichment (Figure 4(g)). The maximal degree of enrichment around 10 minutes qualitatively matches the simulation result shown in Figure 4(d). We conclude that the use of this enrichment module ought to lower the minimum detectable concentration of the overall biosensing process of about 5-fold at the tested concentration.

2.4 Process integration and detection rate evaluation

To characterize the performance of the enrichment system in the context of the whole biosensing process, we conducted measurements of the detection rate (in terms of genome copies loaded on the metal probe) of the combined steps downstream of collection (Figure 1) and quantified any potential losses during the transfer of material from one step to another.

We first evaluated the detection rate when we loaded 500 copies of SARS-CoV-2 viral particles on the metal probe (Figure 5(a)). With this number of copies, we expect that the concentration of the sample, after going through heat extraction and enrichment with the efficiencies we obtained for extraction and enrichment (Figures 3(d) and 4(g)), would be close to the LoD of RT-qPCR (Figure 4(f)). The Ct values of all the replicates are reported in Figure 5(b)(left panel) and show a detection rate of 100% for N=22.

We then sought to explore if we could detect lower than 500 copies. To this end, we conducted another set of experiments in which we loaded 430 copies on the metal probe. The Ct values of all the replicates are reported in Figure 5(b)(middle and right panels). Quantification of detection rate before and after enrichment at 430 copies shows that enrichment boosted the detection rate from 46.7% to 78.6% for N=15 and 14, respectively. For the non-template controls, none of the NTCs were amplified (0/15) (see Table S6. Left: Ct values before enrichment. Right: Ct values after enrichment).

There are several sources of error in our quantification process that could be responsible for underestimating the system's performance. Specifically, the use of the ATCC inactivated virus is one such source

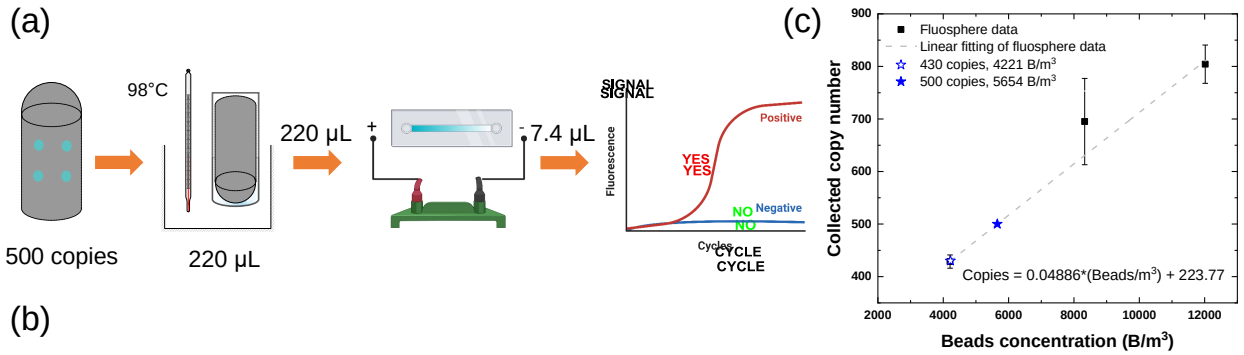

(b)

500 copies (with enrichment)

Rep. #	Ct value	Rep. #	Ct value
1	34.16	12	31.62
2	32.98	13	32.2
3	34.11	14	36.03
4	33.85	15	36.65
5	34.17	16	34.68
6	33.58	17	31.17
7	33.63	18	34.01
8	32.77	19	31.98
9	32.24	20	33.48
10	33.15	21	33.79
11	33.82	22	31.72
Detection rate:		22/22 (100%)	

430 copies (no enrichment)

Rep. #	Ct value	Rep. #	Ct value
1	ND	9	ND
2	36.74	10	ND
3	35.26	11	ND
4	35.28	12	35.33
5	ND	13	36.56
6	ND	14	ND
7	ND	15	36.62
8	34.78		
Detection rate:		7/15 (46.7%)	

430 copies (with enrichment)

Rep. #	Ct value	Rep. #	Ct value
1	36.58	9	36.23
2	36.45	10	33.53
3	35.67	11	31.04
4	33.78	12	36.74
5	33.78	13	36.85
6	ND	14	ND
7	33.58		
8	ND		
Detection rate:		11/14 (78.6%)	

Figure 5: **Evaluation of the detection rate within the whole biosensing process.** (a) **Loading:** the metal probe was loaded with either nuclease-free water (for NTCs) or SARS-CoV-2 ATCC-VP (for biological replicates) in 1 µL droplets with a total volume of 10 µL. **Extraction:** the metal probe was dried in a biosafety cabinet and then collected into a 2 mL tube with 220 µL of water before being heated at 98 °C for 5 minutes. **Enrichment:** the recovered liquid from extraction was supplemented with LA buffer and concentrated in the enrichment device for 10 minutes. **Detection:** 7.4 µL of enriched liquid was extracted from the positive end of the enrichment device and analyzed with RT-qPCR to determine the Ct value. (b) Results of integration test starting with 500 copies (left) and with 430 copies (middle and right). NTCs were all negative and can be found in "Integration" of Supplementary Materials (Table S6). (c) We conducted linear regression analysis over the three data points at the lower in-air concentrations tested in Figure 2(d). The fitted line was used to estimate the in-air concentrations from the two copy numbers (500 and 430) in the integration test.

of error. In fact, being heat-inactivated, many of the RNA molecules are likely already exposed and can be easily damaged during the heat extraction process. This is consistent with our finding that when performing heat extraction in water, we achieved lower efficiency than just analyzing the unheated water with RT-qPCR (Tables S1, S2).

2.5 Estimation of the minimum detectable concentration

Referring to Figure 5(c), the two copy numbers that we evaluated in the integration test, 430 and 500 copies, correspond to an in-air concentration of 4,221 particles/m^3 and 5,654 particles/m^3, respectively. This minimum detectable concentration (MDC) that we estimate here in the presence of RNA enrichment is consistent with the higher MDC characterized previously with the same sampler in the absence of any enrichment [26, 27, 28]. Specifically, the ESP sampler used here was coupled with laboratory post-processing to extract and detect microbes in a containment chamber with approximately 11 colony-forming units(CFU)/ L

of *Bacillus globigii* [26] or with about 37,000 gc/m^3 of influenza virus inside a biosafety cabinet [28]. With RNA enrichment, we thus achieve an MDC that is about 2-7 times lower than that obtained without enrichment.

We also compared the MDC estimated from the integration test to the MDC that we would obtain using formulas (1) and (2) with the experimentally quantified efficiencies for each step of the biosensing process. To this end, all the efficiencies evaluated are characterized by a mean value, $\bar{\eta}_c$, $\bar{\eta}_{ex}$, and $\bar{\eta}_{en}$, and a standard deviation σ_c, σ_{ex}, and σ_{en}, respectively. Specifically, given the evaluations of the efficiencies in Figure 2 ($\eta_c = 0.10 \pm 0.001$), Figure 3 ($\eta_{ex} = 0.115 \pm 0.09$) and Figure 4 ($\eta_{en} = 0.14 \pm 0.02$), the mean value $\bar{\eta}_{tot}$ is given by

$$\bar{\eta}_{tot} = \bar{\eta}_c \cdot \bar{\eta}_{ex} \cdot \bar{\eta}_{en} = 0.00161.$$

The standard variation σ_{tot} of the whole process efficiency can then be evaluated by exploiting the formula for the uncertainty propagation in a product, that is,

$$\sigma_{tot} = \bar{\eta}_{tot} \cdot \sqrt{\left(\frac{\sigma_c}{\bar{\eta}_c}\right)^2 + \left(\frac{\sigma_{ex}}{\bar{\eta}_{ex}}\right)^2 + \left(\frac{\sigma_{en}}{\bar{\eta}_{en}}\right)^2} \approx 0.00127. \tag{3}$$

From this, the mean concentration in air that we can detect is $\bar{C}_{min} := \mathrm{LoD} \cdot V_{\mathrm{PCR}}/\bar{\eta}_{tot} = 0.25 \cdot 20/0.00161 \approx 3106$ particles/m^3. From this calculation, it is possible to conclude that the minimum concentration C_{min} that our device is able to detect is between 649 and 5,562 particles/m^3, which is consistent with the in-air concentrations of 4,221 and 5,654 particles/m^3 found with the integration test at a detection rate of 78.6% and 100%, respectively.

3 Conclusions

The ultra-low concentrations of virus in the air (as low as 5,000 genome copies (gc)/m^3 in some cases [22, 39]) when compared to those in nasal swabs of sick patients ($10^4 - 10^7$gc/mL [43]) pose a unique challenge to the biosensing problem. Existing technologies could only detect at concentrations as high as 31,800 gc/m^3 [23]. This discrepancy highlights the need for more sensitive biosensing methods capable of detecting common pathogens at the lower in-air concentrations. We characterized in a laboratory setting the performance of an RT-qPCR-based biosensing process incorporating an electrophoretic step for nucleic acid enrichment and reached a minimum detectable concentration of about 5,000 gc/m^3, a concentration that falls in the lower range of influenza virus and SARS-CoV-2 concentrations reported in the literature [39, 22]. Utilization of lyophilized RT-qPCR reagents [44] could help us avoid the dilution in forming the PCR reaction volume and further lower our minimum detectable concentration by up to a factor of three leading to $\bar{C}_{min} \approx 2,000$ gc/m^3.

Our process was integrated with pathogen collection using a compact, inexpensive, ESP air sampler, as a stand-alone system for early detection of airborne pathogens. The ESP sampler can collect more concentrated sample due to small extraction liquid volume, while the cyclone sampler used in other studies [45, 46] obtained a higher total number of particles in a more dilute solution [26]. To extract the viral RNA, we implemented a simple heat-extraction protocol to circumvent the need for commercial extraction kits, overall making the platform field-ready and relatively inexpensive. Following heat extraction, we developed and characterized an enrichment system which uses small channel electrophoresis against a semipermeable membrane. This system is able to concentrate RNA by nearly 5-fold in just 10 minutes.

Here, we designed the enrichment device to be simple, inexpensive, and fieldable, but incorporation of parallelized microcapillaries, fluidic manifolds [47], electric field gradient focusing, or isotachophoresis [48, 49] could further improve the degree of enrichment at the expense of additional cost and complexity. Compared to an on-chip isotachophoresis approach [49], our membrane-coupled enrichment process easily allows for concentration and detection of synthetic viral RNA samples with tenfold lower concentration while employing simpler buffers and equipment. This also mitigates hardware reliance and brings the consumable cost down to below \$1/test, much lower compared to the \$6-\$10/test when using commercially available extraction and concentration kits. The process that we have proposed, being based on RT-qPCR detection, is applicable to any virus whose genetic sequence is known. At the same time, our enrichment process can be used to concentrate samples in a number of other applications including nucleic acid fragment analysis and quality control, next-generation sequencing, and general biomolecular analysis.

4 Methods

4.1 Materials

Heat-inactivated SARS-CoV-2 (strain 2019-nCoV/USA-WA1/2020, VR-1986HK) and Quantitative synthetic SARS-CoV-2 RNA were obtained from ATCC (Lot numbers: 70037781 & 70048443). The Luna Universal One-Step RT-qPCR kit (New England BioLabs, E3005) was utilized for all RT-qPCRs in a Roche LightCycler 480. N2 forward (IDT, 10006824, 5'-TTACAAACATTGGCCGCAAA-3') and N2 reverse (IDT, 10006825, 5'-GCGCGACATTCCGAAGAA-3') primers were utilized in all reactions. Fluorescent beads (F13081), CountBright Absolute Counting Beads (Invitrogen, C36950), and SYBR Safe™ Stain (GeneRuler 1kb DNA Ladder, SM0312) were obtained from ThermoFisher.

4.2 Collection

The air sampling experiments were conducted inside a containment tent (Abetement Technologies, AG3000-MCCK) (Figure 2(b),(c)), in which solutions of 1 µm diameter fluorescent beads at varying concentrations (FluoSpheres - Thermo Fisher, F13081) were nebulized. Refer to Section 2.1 for the rationale behind choosing 1 µm beads. We selected the portable ESP air sampler developed by De Sousa et al. [26, 27]. Specifically, we diluted the fluorescent beads in filtered deionized water to the desired concentrations and nebulized in the tent through four Omron nebulizers located at the four top corners of the tent. The aerosol sampler was located in the tent in a central position, 20 cm from the ground and 1.5 m from the nebulizers (Figure 2(c)). In each experiment, we considered a continuous but small rate of 0.3 mL / min of nebulization and a simultaneous collection. All experiments lasted $T = 22$ min. At the end of sampling, the metal probe was transferred into a 2 mL microcentrifuge tube and 250 µL of filtered water was added. After vortexing the tube for 1 min, the metal probe was removed with a magnet and put in a new 2 mL microcentrifuge tube. Another 250 µL of filtered water was added, and the tube was again vortexed for 1 min. We used a BD Accuri C6 flow cytometer to quantify the amount of fluorescent beads in all the tubes, representing the total number of fluorescent beads collected on the probe (See "Collection" in Supplementary Materials for details).

4.3 Heat extraction

We chose the heat-inactivated SARS-CoV-2, hereafter referred to as ATCC-VP, as a quantitative control in molecular assays and to evaluate the efficiency of several workflows, with the advantage of requiring only a BL2 lab [50, 51]. For characterizing the efficiency of the heat extraction process, we artificially loaded a known amount of virus on the metal probe, performed heat extraction, and then transferred 7.4 µL to a 20 µL RT-qPCR reaction. Before the start of each extraction test, the metal probes were thoroughly cleaned to eliminate any contamination by RNA or RNase (see "Metal collector cleaning (molecular biology grade)" in Supplementary Materials). In the biosafety cabinet, we loaded 10 µL of diluted solution of ATCC-VP on the probe in ten 1 µL droplets evenly distributed (see "Heat Extraction" in Supplementary Materials). After loading, we recollected the metal probe into a 2 mL microcentrifuge tube, added in 220 µL of nuclease-free water, and ensured the entire metal surface was immersed (Figure 3(a)).

To release RNA from the viral particles, we placed the tube containing the metal probe in an OniLAB Mini Dry Bath Incubator preheated to 98 °C and incubated for 5 minutes [52, 40], as illustrated in Figure 3(a). After incubation, the tube was immediately transferred to ice and kept there for 5 minutes. Then, we removed the metal probe from the tube with a magnet, and used a pipette to collect residual droplets adhering to the surface of the metal probe to maximize recovery. Typically, about 210 µL could be recovered out of the 220 µL input volume. We then used a volume of 7.4 µL to prepare a 20 µL RT-qPCR reaction targeting SARS-CoV-2 RNA. The number of genome copies were obtained by comparing the Ct values with standard samples using synthetic SARS-CoV-2 RNA (see Figure 3(b)). We quantified the extraction efficiency as the ratio of recovered genome copies, calculated from the Ct values of RT-qPCR using the standard curve, and the total number of copies loaded on the metal probe, calculated from serial dilutions of the original stock with concentrations specified by the manufacturer (following the definition in Figure 3(c)).

4.4 RNA enrichment and quantification

To test the performance of the enrichment device, synthetic SARS-CoV-2 RNA (ATCC, VR-3276SD) was diluted to a target concentration of 1.2 copies / µL in 250 µL of 5 mM lithium acetate (LA) buffer optimized for fast electrophoresis and minimal Joule heating [42]. After addition of the RNA to the buffer, the sample was homogenized by pipetting. Before loading the PDMS devices, a portion of the sample was set aside on ice for RT-qPCR analysis. Devices were loaded with sample by injection using a syringe. Briefly, two 23 gauge needles (BD, 305194) were pierced through the PDMS adjacent to each membrane. One needle was used to fill the channel by steady injection of a 250 µL sample from a syringe, while the other needle served as an air escape. Following injection of the sample, any bubbles created were collected near the air escape needle and removed with a syringe, allowing fluid from the sample injection needle to replace the volume. The needles were then removed, leaving no visible holes in the PDMS.

After loading, the devices were placed in a standard benchtop gel electrophoresis bath (VWR, 89032-290) with a 15.25 cm distance between electrodes filled with 5 mM LA running buffer. Devices were aligned to place the axis of the channel parallel to the direction of the electric field (Figure 4a). All tests were conducted using a voltage of 300 V (voltage supply dimensions = 200 x 290 x 70 mm (W x D x H), weight = 1.2 kg), corresponding to an approximate electric field strength of 2,000 V/m or 20 V/cm. Enrichment was allowed to proceed for 5, 10, or 15 minutes.

Upon completion of electrophoresis, devices were gently removed from the running bath and a sample of 7.4 µL was extracted manually using the following procedure. A 23-gauge needle was first inserted into the channel near the negative-terminal membrane to provide a fluid escape. To separate the most concentrated 7.4 µL from the remaining 242.6 µL of fluid, a small air gap was inserted with a syringe into the channel at a distance of 1.6 mm from the positive-terminal membrane. The channel was then cut with a razor blade across the air gap, and the 7.4 µL sample was removed using a micropipette and analyzed by RT-qPCR to quantify the concentration of SARS-CoV-2 RNA relative to unenriched control samples. The PDMS chip can also be outfitted with inlet and outlet tubing for automatic recovery of the enriched sample.

4.5 RT-qPCR detection

The Luna Universal One-Step RT-qPCR kit (NEB, E3005) was utilized for all RT-qPCRs in a Roche LightCycler 480. We used serial dilutions of quantitative synthetic SARS-CoV-2 RNA at known concentrations for detection with RT-qPCR. For each concentration, 24 replicates of SARS-CoV-2 RNA diluted in either nuclease-free water or LA buffer were tested for detection. Respectively, 24 replicates of non-template controls (NTCs) in either nuclease-free water or LA buffer were also tested. N2 primers [53] were utilized in all RT-qPCR reactions.

4.6 Integration

To place the performance of the enrichment device into the context of the whole biosensing process, we directly loaded the metal probe with heat-inactivated SARS-CoV-2 viral particles and carried out heat-extraction, enrichment, and detection (Figure 5(a)). We define the limit-of-detection (LoD) to be the lowest genome copies loaded on the metal probe at which the detection rate stays above 95%. Therefore, we first evaluated the detection rate at 500 starting genome copies on the metal probe, and then explored a lower number of copies of 430. For the 430 copies, we followed two parallel routes after heat extraction to evaluate the benefit of incorporating the enrichment process for detection. Specifically, in the first route, we aliquoted 7.4 µL from the recovered solution (averaged 210 µL) and made a 20 µL RT-qPCR reaction to analyze (no enrichment). The rest of the solution was supplemented with 13 µL of PCR-grade LA buffer stock (20x) and nuclease-free water to make a total input volume of 250 µL to the enrichment process (Figure S6). Because of the extraction of this 7.4 µL, we effectively removed 15 copies, leaving us with 415 copies. Also, due to a loss of 0.5% of the volume during loading 1 µL droplets, we eventually reached an equivalent starting number of 394 particles, which implies that we are underestimating our performance (see "Integration" in Supplementary Materials). For the non-template controls, we loaded the metal probe with 10 µL of nuclease-free water and went through the same process as we did for the 430 copies case.

Acknowledgements

The authors would like to acknowledge Mehdi Salek, Linda Griffith, Kurt Broderick, and the MIT NEET Living Machines program for assistance with the development of the enrichment module, Dan Gilbert at the MIT Laboratory for Manufacturing and Productivity for assistance with device fabrication, and the MIT BioMicro Center and the labs of Richard Young and Ron Weiss for assistance with RT-qPCR. The authors thank the lab of Nicholas Fang for the help with the COMSOL software simulations, as well as Krishna Manoj, Ted Grunberg, and Miranda Cai for assistance with early prototypes and helpful discussions. We thank the Deshpande Center, the NSF Graduate Research Fellowship (grant number 1745302 to K.J.O), and the Air Force Office of Scientific Research (grant number FA9550-20-1-0044) for funding support.

Competing Interest Statement

The Massachusetts Institute of Technology has filed a patent application based on this study. The authors declare no other competing interests.

References

[1] Centers for Disease Control and Prevention, "Revised U.S. Surveillance Case Definition for Severe Acute Respiratory Syndrome (SARS) and Update on SARS Cases — United States and Worldwide, December 2003," 2003.

[2] Centers for Disease Control and Prevention, "The 2009 H1N1 Pandemic: Summary Highlights, April 2009-April 2010," 2009.

[3] Centers for Disease Control and Prevention, "Severe Respiratory Illness Associated with Middle East Respiratory Syndrome Coronavirus (MERS-CoV) — Worldwide, 2012–2013," 2013.

[4] Centers for Disease Control and Prevention, "CDC Releases Detailed History of the 2014-2016 Ebola Response in MMWR," 2016.

[5] H. M. Biggs, X. Lu, L. Dettinger, S. Sakthivel, J. T. Watson, and S. W. Boktor, " Adenovirus-associated influenza-like illness among college students, Pennsylvania, USA," *Emerging Infectious Diseases*, vol. 24, no. 11, p. 2117, 2018.

[6] Z. Peng, A. P. Rojas, E. Kropff, W. Bahnfleth, G. Buonanno, S. J. Dancer, J. Kurnitski, Y. Li, M. G. Loomans, L. C. Marr, *et al.*, "Practical indicators for risk of airborne transmission in shared indoor environments and their application to COVID-19 outbreaks," *Environmental Science & Technology*, vol. 56, no. 2, pp. 1125–1137, 2022.

[7] C. L. Hansen, S. S. Chaves, C. Demont, and C. Viboud, "Mortality associated with influenza and respiratory syncytial virus in the US, 1999-2018," *JAMA network open*, vol. 5, no. 2, pp. e220527–e220527, 2022.

[8] S. Yan, D. Weycker, and S. Sokolowski, "US healthcare costs attributable to type A and type B influenza," *Human vaccines & immunotherapeutics*, vol. 13, no. 9, pp. 2041–2047, 2017.

[9] Y. Choi, A. Hill-Ricciuti, A. R. Branche, W. D. Sieling, L. Saiman, E. E. Walsh, M. Phillips, A. R. Falsey, and L. Finelli, "Cost determinants among adults hospitalized with respiratory syncytial virus in the United States, 2017–2019," *Influenza and Other Respiratory Viruses*, vol. 16, no. 1, pp. 151–158, 2022.

[10] Y.-J. Chen and J.-T. Huang, "Development of a portable bioaerosol capture device for influenza virus detection," *Biosensors and Bioelectronics: X*, vol. 13, p. 100316, 2023.

[11] I. M. Blake, P. Chenoweth, H. Okayasu, C. A. Donnelly, R. B. Aylward, and N. C. Grassly, "Faster detection of poliomyelitis outbreaks to support polio eradication," *Emerging Infectious Diseases*, vol. 22, no. 3, p. 449, 2016.

[12] B. Impouma, M. Roelens, G. S. Williams, A. Flahault, C. T. Codeço, F. Moussana, B. Farham, E. L. Hamblion, F. Mboussou, and O. Keiser, "Measuring timeliness of outbreak response in the World Health Organization African region, 2017–2019," *Emerging Infectious Diseases*, vol. 26, no. 11, p. 2555, 2020.

[13] Resolve to Save Lives, "Timeliness metrics: an opportunity for epidemic response tracking and improvement," 2021.

[14] S. F. Fitzgerald, G. Rossi, A. S. Low, S. P. McAteer, B. O'Keefe, D. Findlay, G. J. Cameron, P. Pollard, P. T. Singleton, G. Ponton, *et al.*, "Site specific relationships between COVID-19 cases and SARS-CoV-2 viral load in wastewater treatment plant influent," *Environmental Science & Technology*, vol. 55, no. 22, pp. 15276–15286, 2021.

[15] A. J. Hay and J. W. McCauley, "The who global influenza surveillance and response system (gisrs)—a future perspective," *Influenza and other respiratory viruses*, vol. 12, no. 5, pp. 551–557, 2018.

[16] M. Chadha, S. Hirve, C. Bancej, I. Barr, E. Baumeister, B. Caetano, M. Chittaganpitch, B. Darmaa, J. Ellis, R. Fasce, *et al.*, "Human respiratory syncytial virus and influenza seasonality patterns—early findings from the who global respiratory syncytial virus surveillance," *Influenza and other respiratory viruses*, vol. 14, no. 6, pp. 638–646, 2020.

[17] The Novel Coronavirus Pneumonia Emergency Response Epidemiology Team, "The Epidemiological Characteristics of an Outbreak of 2019 Novel Coronavirus Diseases (COVID-19) — China, 2020," *China CDC Weekly*, vol. 2, p. 113, 2020.

[18] C. Faes, S. Abrams, D. Van Beckhoven, G. Meyfroidt, E. Vlieghe, N. Hens, and B. C. G. on COVID-19 Hospital Surveillance, "Time between symptom onset, hospitalisation and recovery or death: statistical analysis of Belgian COVID-19 patients," *International Journal of Environmental Research and Public Health*, vol. 17, no. 20, p. 7560, 2020.

[19] Centers for Disease Control and Prevention, "Overview of Testing for SARS-CoV-2, the virus that causes COVID-19," 2023.

[20] C. Chen, C. Zhu, D. Yan, H. Liu, D. Li, Y. Zhou, X. Fu, J. Wu, C. Ding, G. Tian, *et al.*, "The epidemiological and radiographical characteristics of asymptomatic infections with the novel coronavirus (COVID-19): a systematic review and meta-analysis," *International Journal of Infectious Diseases*, vol. 104, pp. 458–464, 2021.

[21] National Research Council, *BioWatch and public health surveillance: Evaluating systems for the early detection of biological threats: Abbreviated version*. National Academies Press, 2011.

[22] J. A. Lednicky, M. Lauzardo, Z. H. Fan, A. Jutla, T. B. Tilly, M. Gangwar, M. Usmani, S. N. Shankar, K. Mohamed, A. Eiguren-Fernandez, *et al.*, "Viable SARS-CoV-2 in the air of a hospital room with COVID-19 patients," *International Journal of Infectious Diseases*, vol. 100, pp. 476–482, 2020.

[23] P. F. Horve, L. Dietz, D. Northcutt, J. Stenson, and K. Van Den Wymelenberg, "Evaluation of a bioaerosol sampler for indoor environmental surveillance of Severe Acute Respiratory Syndrome Coronavirus 2," *PLoS One*, vol. 16, no. 11, p. e0257689, 2021.

[24] A. H. Abeykoon, M. Poon, S. M. Firestone, M. A. Stevenson, A. K. Wiethoelter, and G. A. Vincent, "Performance Evaluation and Validation of Air Samplers To Detect Aerosolized Coxiella burnetii," *Microbiology Spectrum*, vol. 10, no. 5, pp. e00655–22, 2022.

[25] I. Lee, Y. Seok, H. Jung, B. Yang, J. Lee, J. Kim, H. Pyo, C.-S. Song, W. Choi, M.-G. Kim, *et al.*, "Integrated bioaerosol sampling/monitoring platform: field-deployable and rapid detection of airborne viruses," *ACS sensors*, vol. 5, no. 12, pp. 3915–3922, 2020.

[26] N. Rufino de Sousa, N. Sandström, L. Shen, K. Håkansson, R. Vezozzo, K. Udekwu, J. Croda, and A. Rothfuchs, "A fieldable electrostatic air sampler enabling tuberculosis detection in bioaerosols," *Tuberculosis*, vol. 120, p. 101896, 12 2019.

[27] N. Rufino de Sousa, L. Steponaviciute, L. Margerie, K. Nissen, M. Kjellin, B. Reinius, E. Salaneck, K. I. Udekwu, and A. G. Rothfuchs, "Detection and isolation of airborne SARS-CoV-2 in a hospital setting," *Indoor Air*, vol. 32, no. 3, p. e13023, 2022.

[28] L. Ladhani, G. Pardon, H. Meeuws, L. van Wesenbeeck, K. Schmidt, L. Stuyver, and W. van der Wijngaart, "Sampling and detection of airborne influenza virus towards point-of-care applications," *PloS one*, vol. 12, no. 3, p. e0174314, 2017.

[29] H. R. Kim, S. An, and J. Hwang, "An integrated system of air sampling and simultaneous enrichment for rapid biosensing of airborne coronavirus and influenza virus," *Biosensors and Bioelectronics*, vol. 170, p. 112656, 2020.

[30] K. Pardee, A. A. Green, M. K. Takahashi, D. Braff, G. Lambert, J. W. Lee, T. Ferrante, D. Ma, N. Donghia, M. Fan, *et al.*, "Rapid, low-cost detection of Zika virus using programmable biomolecular components," *Cell*, vol. 165, no. 5, pp. 1255–1266, 2016.

[31] M. Karlikow, S. J. R. da Silva, Y. Guo, S. Cicek, L. Krokovsky, P. Homme, Y. Xiong, T. Xu, M.-A. Calderón-Peláez, S. Camacho-Ortega, *et al.*, "Field validation of the performance of paper-based tests for the detection of the Zika and chikungunya viruses in serum samples," *Nature Biomedical Engineering*, vol. 6, no. 3, pp. 246–256, 2022.

[32] C. C. Wang, K. A. Prather, J. Sznitman, J. L. Jimenez, S. S. Lakdawala, Z. Tufekci, and L. C. Marr, "Airborne transmission of respiratory viruses," *Science*, vol. 373, no. 6558, p. eabd9149, 2021.

[33] V. Groma, S. Kugler, Á. Farkas, P. Füri, B. Madas, A. Nagy, T. Erdélyi, A. Horváth, V. Müller, R. Szántó-Egész, *et al.*, "Size distribution and relationship of airborne SARS-CoV-2 RNA to indoor aerosol in hospital ward environments," *Scientific Reports*, vol. 13, no. 1, p. 3566, 2023.

[34] S. A. Hawks, A. J. Prussin, S. C. Kuchinsky, J. Pan, L. C. Marr, and N. K. Duggal, "Infectious SARS-CoV-2 is emitted in aerosol particles," *MBio*, vol. 12, no. 5, pp. e02527–21, 2021.

[35] Y. Liu, Z. Ning, Y. Chen, M. Guo, Y. Liu, N. K. Gali, L. Sun, Y. Duan, J. Cai, D. Westerdahl, *et al.*, "Aerodynamic analysis of SARS-CoV-2 in two Wuhan hospitals," *Nature*, vol. 582, no. 7813, pp. 557–560, 2020.

[36] E. M. Mahabee-Gittens, A. L. Merianos, and G. E. Matt, "Letter to the editor regarding:"an imperative need for research on the role of environmental factors in transmission of novel coronavirus (COVID-19)"—secondhand and thirdhand smoke as potential sources of COVID-19," *Environmental Science & Technology*, vol. 54, no. 9, pp. 5309–5310, 2020.

[37] M. Alsved, D. Nygren, S. Thuresson, C.-J. Fraenkel, P. Medstrand, and J. Löndahl, "Size distribution of exhaled aerosol particles containing SARS-CoV-2 RNA," *Infectious Diseases*, vol. 55, no. 2, pp. 158–163, 2023.

[38] Omron Healthcare, "Compressor Nebulizer Model NE-C801-Instruction Manual," 2021.

[39] W. Yang, S. Elankumaran, and L. C. Marr, "Concentrations and size distributions of airborne influenza A viruses measured indoors at a health centre, a day-care centre and on aeroplanes," *Journal of the Royal Society Interface*, vol. 8, no. 61, pp. 1176–1184, 2011.

[40] J. K. Jung, K. K. Alam, M. S. Verosloff, D. A. Capdevila, M. Desmau, P. R. Clauer, J. W. Lee, P. Q. Nguyen, P. A. Pastén, S. J. Matiasek, *et al.*, "Cell-free biosensors for rapid detection of water contaminants," *Nature Biotechnology*, vol. 38, no. 12, pp. 1451–1459, 2020.

[41] A. Parra-Guardado, C. Sweeney, E. Hayes, B. Trueman, Y. Huang, R. Jamieson, J. Rand, G. Gagnon, and A. Stoddart, "Development of a rapid pre-concentration protocol and a magnetic beads-based rna extraction method for sars-cov-2 detection in raw municipal wastewater," *Environmental Science: Water Research & Technology*, vol. 8, no. 1, pp. 47–61, 2022.

[42] J. R. Brody, E. S. Calhoun, E. Gallmeier, T. D. Creavalle, and S. E. Kern, "Ultra-fast high-resolution agarose electrophoresis of DNA and RNA using low-molarity conductive media," *Biotechniques*, vol. 37, no. 4, pp. 598–602, 2004.

[43] A. Mawaddah, H. S. Genden, S. G. Lum, and M. B. Marina, "Upper respiratory tract sampling in COVID-19," *The Malaysian journal of pathology*, vol. 42, no. 1, pp. 23–35, 2020.

[44] Y. Xu, J. G. Borgaro, G. Ren, K. B. Vrtis, G. C. Patton, and N. M. Nichols, "Optimized conditions for the CDC Influenza SARS-CoV-2 (Flu SC2) Multiplex Assay using Luna® One-Step RT-qPCR Reagents," *Rn*, vol. 107, no. 106, p. 106.

[45] J. V. Puthussery, D. P. Ghumra, K. R. McBrearty, B. M. Doherty, B. J. Sumlin, A. Sarabandi, A. G. Mandal, N. J. Shetty, W. D. Gardiner, J. P. Magrecki, *et al.*, "Real-time environmental surveillance of SARS-CoV-2 aerosols," *Nature Communications*, vol. 14, no. 1, p. 3692, 2023.

[46] F. Lu, O. Gecgel, A. Ramanujam, and G. G. Botte, "SARS-CoV-2 Surveillance in Indoor Air Using Electrochemical Sensor for Continuous Monitoring and Real-Time Alerts," *Biosensors*, vol. 12, no. 7, p. 523, 2022.

[47] W. Qiao, C. Wang, Z. Ding, and et al, "A two-stage electrophoretic microfluidic device for nucleic acid collection and enrichment," *Microfluidics and Nanofluidics*, no. 77, 2016.

[48] G. Garcia-Schwarz, A. Rogacs, S. Bahga, and J. Santiago, "On-chip isotachophoresis for separation of ions and purification of nucleic acids.," *J Vis Exp.*, p. e3890, 2012.

[49] A. Ramachandran, D. Huyke, E. Sharma, M. Sahoo, C. Huang, N. Banaei, B. Pinsky, and J. Santiago, " Electric field-driven microfluidics for rapid CRISPR-based diagnostics and its application to detection of SARS-CoV-2," *PNAS*, no. 47, pp. 29518–29525, 2020.

[50] K. T. Ash, Y. Li, I. Alamilla, D. C. Joyner, D. E. Williams, P. McKay, B. Green, C. Iler, S. DeBlander, C. North, *et al.*, "SARS-CoV-2 raw wastewater surveillance from student residences on an urban university campus," *Frontiers in Microbiology*, vol. 14, p. 1101205, 2023.

[51] B. J. Huge, D. North, C. B. Mousseau, K. Bibby, N. J. Dovichi, and M. M. Champion, "Comparison of RT-dPCR and RT-qPCR and the effects of freeze–thaw cycle and glycine release buffer for wastewater SARS-CoV-2 analysis," *Scientific Reports*, vol. 12, no. 1, p. 20641, 2022.

[52] B. Guan, K. M. Frank, J. O. Maldonado, M. Beach, E. Pelayo, B. M. Warner, and R. B. Hufnagel, "Sensitive extraction-free SARS-CoV-2 RNA virus detection using a chelating resin," *Iscience*, vol. 24, no. 9, p. 102960, 2021.

[53] X. Lu, L. Wang, S. Sakthivel, B. Whitaker, J. Murray, S. Kamili, B. Lynch, L. Malapati, J. Burke, J. Harcourt, A. Tamin, J. Thornburg, J. Villanueva, and S. Lindstrom, "US CDC Real-Time Reverse Transcription PCR Panel for Detection of Severe Acute Respiratory Syndrome Coronavirus 2," *Emerging Infectious Diseases*, vol. 26, no. 8, pp. 1654–1665, 2020.

[54] H. Wang, S. Lu, J. Cheng, and Z. J. Zhai, "Inverse modeling of indoor instantaneous airborne contaminant source location with adjoint probability-based method under dynamic airflow field," *Building and Environment*, vol. 117, pp. 178–190, 2017.

[55] T. Zhang and Q. Chen, "Identification of contaminant sources in enclosed spaces by a single sensor," *Indoor air*, vol. 17, no. 6, pp. 439–449, 2007.

[56] Q. Feng, H. Cai, F. Li, X. Liu, S. Liu, and J. Xu, "An improved particle swarm optimization method for locating time-varying indoor particle sources," *Building and Environment*, vol. 147, pp. 146–157, 2019.

[57] Alconox Inc., "Tech notes: Cleaning Proteins, RNA and DNA from Lab Equipment," 2020.

[58] R. A. Khailany, M. Safdar, and M. Ozaslan, "Genomic characterization of a novel SARS-CoV-2," *Gene reports*, vol. 19, p. 100682, 2020.

[59] Y. Song, C. Wang, J. Li, and D. Li, "Vortex generation in electroosmotic flow in a straight polydimethylsiloxane microchannel with different polybrene modified-to-unmodified section length ratios," *Microfluidics and Nanofluidics*, vol. 23, pp. 1–11, 2019.

[60] R. Peng and D. Li, "Electroosmotic flow in single PDMS nanochannels," *Nanoscale*, vol. 8, no. 24, pp. 12237–12246, 2016.

[61] I.-C. Yeh and G. Hummer, "Diffusion and electrophoretic mobility of single-stranded RNA from molecular dynamics simulations," *Biophysical Journal*, vol. 86, no. 2, pp. 681–689, 2004.

[62] N. C. Stellwagen, S. Magnusdottir, C. Gelfi, and P. G. Righetti, "Measuring the translational diffusion coefficients of small DNA molecules by capillary electrophoresis," *Biopolymers: Original Research on Biomolecules*, vol. 58, no. 4, pp. 390–397, 2001.

[63] A. E. Nkodo, J. M. Garnier, B. Tinland, H. Ren, C. Desruisseaux, L. C. McCormick, G. Drouin, and G. W. Slater, "Diffusion coefficient of DNA molecules during free solution electrophoresis," *Electrophoresis*, vol. 22, no. 12, pp. 2424–2432, 2001.

[64] B. Dutagaci, G. Nawrocki, J. Goodluck, A. A. Ashkarran, C. G. Hoogstraten, L. J. Lapidus, and M. Feig, "Charge-driven condensation of RNA and proteins suggests broad role of phase separation in cytoplasmic environments," *Elife*, vol. 10, p. e64004, 2021.

5 Supplementary Materials

Inactivated viral particles

Heat-inactivated SARS-CoV-2 (strain 2019-nCoV/USA-WA1/2020, VR-1986HK) was obtained from ATCC, Lot number: 70037781. This material has been inactivated by heating at 65 °C for 30 minutes, and we aliquoted the original stock upon receipt to minimize the number of freeze-thaw cycles and ensure consistency by using one of the same batch of aliquoted samples for each experiment.

Synthetic SARS-CoV-2 RNA

Quantitative synthetic SARS-CoV-2 RNA was obtained from ATCC (VR-3276SD, lot number: 70048443) and used as standard controls for characterization of the RT-qPCR assay, and evaluation of the performance of the electrophoresis enrichment system. The synthetic RNA contains fragments from the ORF1ab, E, and N regions of the SARS-CoV-2 genome.

Process efficiencies

We define the collection efficiency η_c as the ratio between the number of particles collected on the metal probe and the number of particles per m^3 of air. The extraction efficiency η_{ex} is defined as the ratio between the number of RNA copies extracted in 220 µL of water and the number of viral particles loaded on the metal probe. The enrichment efficiency η_{en} is the ratio between the number of RNA molecules in the enriched fraction of the volume extracted (7.4 µL) and the number of RNA molecules in the enrichment device volume (250 µL).

Collection

The electrostatic precipitator (ESP) device is made of a sealed-plastic enclosure (13x13x7.5 cm), with four carbon brush ionizers at the four corners of the upper surface and a magnetic holder in the center of the upper surface. The collector, a stainless-steel metal probe (3.5 cm in length and 0.88 cm in diameter), is magnetically attached to the holder. The ionizers are electrically connected to the negative output voltage of a -20 kV high-voltage supply located within the device, while the magnetic holder is electrically grounded. While in use, the ESP creates a strong electric field between the ionizers and the metal probe, which results in the generation of a corona discharge at the tips of the ionizers. Consequently, electrons are emitted in close proximity to the ionizers' tips, causing the ionization of airborne particles nearby. The electric field between the ionizers and the collector thus accelerates the ionized particles towards the metal probe, where they collide, lose their charge, and are ultimately collected. When compared to a pump, an ESP sampler is substantially cheaper, does not produce noise, and only minimally disrupts the airflow, which is an advantage when combining sensing with computational fluid dynamic (CFD) models to estimate particle concentration distributions within a room [54, 55, 56].

After air sampling is completed, the flow cytometry analysis is performed using BD Accuri C6 flow cytometer (BD Biosciences, San Jose, CA). In order to accurately determine the absolute counts of particles in the samples, a known quantity of counting beads (CB) (CountBright Absolute Counting Beads - Invitrogen, C36950) is added to the sample before flow cytometry analysis. CountBright Absolute Counting Beads are a calibrated suspension containing a known concentration of fluorescent microspheres. This allows us to analyze a fraction of the sample volume and precisely determine the total number of particles in our samples using the following formula:

$$\text{Particles}_{\text{total}} = \frac{CB_{\text{total}}}{CB_{\text{Volume analyzed}}} \cdot \text{Particles}_{\text{Volume analyzed}} \tag{4}$$

We also conducted background measurements using only deionized water for nebulization, and reported the results in Figure S1.

Metal collector cleaning (0.5% hydrogen peroxide)

The metal collectors were manufactured at machine shops. CNC (computer numerical control) machine coolant or oily residues on the surface of the metal probe could interfere with the electrostatic precipitation

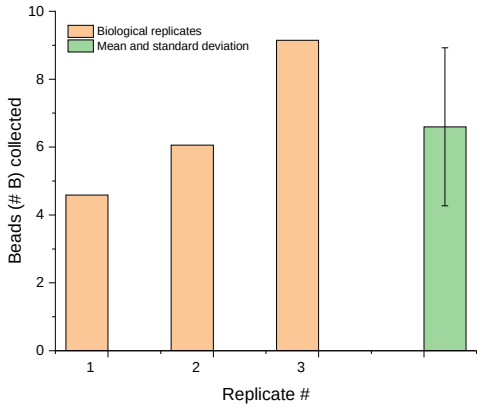

Figure S1: **FluoSpheres background measurement.** We performed three replicates of the background measurement in the Collection experiments, where we nebulized DI water without any FluoSpheres added for the same 22 minutes. The metal collectors were treated in the same way as described in Methods: Collection.

and negatively affect the performance of the collection. In order to optimize the process, we placed the metal collectors in the sonicator with MiliQ water, and then ran the sonicator for 20 minutes. We then treated the surface of the metal collectors with the PREempt RTU disinfectant solution that contains 0.5% hydrogen peroxide by soaking overnight. Prior to each Collection test, we used a magnet and a PREempt Wipe to take a clean probe out of PREempt Solution, with no contact with the metal piece directly. Then we used the same wipe to rub the entire surface of that metal piece thoroughly (making sure that the PREempt solution residue is uniform on the surface), then put it on the ESP device. This is because the hydrogen peroxide in the PREempt™solution promotes the generation of free radicals and improves the efficiency of electrostatic precipitators. Then, we sealed the tent and let the metal collector dry in air for 5 minutes before plugging in the nebulizers and ESP device at the same time to inititate collection.

Metal collector cleaning (molecular biology grade)

Before each integration and heat-extraction test, each metal collector was immersed in 1% Alconox™ Detojet™ Low-Foaming Liquid Detergent for overnight. This ensures that any residual RNA would be chemically degraded [57]. After that, the metal collectors were rinsed thoroughly in nuclease-free water three times until no visible foams can be seen. Then, we used the RNaseZap™ RNase Decontamination Solution to spray over the metal collectors. The solution was kept in contact with the metal collectors for 5 minutes, before they were thoroughly rinsed in nuclease-free water another three times until no visible bubbles could be seen. This prevented any potential RNase contamination. The metal collectors were then autoclaved using the sterilize + dry cycle to further keep them dry and clean. The metal collectors' container was then sealed and opened only within a biosafety cabinet.

Heat extraction

To prepare solutions containing a specific number of genome copies of viral particles, we performed a series of 10-fold dilutions of the heat-inactivated SARS-CoV-2. As the stock contains cell lysate and supernatant from Vero E6 cells which were used by the manufacturer to propagate the viruses, special care was taken to sufficiently mix at each step of dilution by pipetting up and down over 50 times in low-binding tubes. At the end of dilution, we aliquoted 10 µL of solution containing targeted numbers of genome copies of the virus as calculated from the original concentration specified by manufacturer. The aliquoting of 10 µL ensured we were loading the same number of genome copies across all biological replicates and improved our consistency (see Figure S2).

The loading of the aliquoted solution onto the metal collector was performed in a biosafety cabinet. We placed one clean metal collector in the center of the cabinet and turned off the air flow. The 10 µL solution

	No heat (on probe)	98 °C, (on probe)						No heat (in water)	98 °C (inwater)
Biological replicate #	-	1	2	3	4	5	6	-	-
Technical replicate #1	34.12	35.05	36.07	33.18	36.21	32.42	ND	31.13	31.78
Technical replicate #2	34.32	33.91	35.23	33.13	34.36	32.68	36.04	32.10	31.23
Technical replicate #3	33.62	33.85	35.90	33.50	35.43	33.48	36.09	31.15	32.17
Technical replicate #4	35.94	33.24	35.21	32.90	35.09	33.01	36.02	31.76	32.75
Mean	34.50	34.01	35.60	33.18	35.27	32.90	36.05	31.54	31.98
Standard deviation	1.00	0.76	0.45	0.25	0.77	0.46	0.04	0.48	0.64
Diluted concentration (cp/µL)	0.34	0.47	0.16	0.82	0.20	0.99	0.12	2.47	1.83
Initial concentration	0.91	1.26	0.43	2.21	0.54	2.67	0.32	6.67	4.94
Efficiency (%)	8.42	11.68	4.02	20.47	5.01	24.71	2.97	61.70	45.68

Table S1: **Results of of heat-extraction tests (2378 copies).** For each biological/technical replicate, the Ct value was reported. The first column was loading the same number of copies on the probe but with no heating treatment, followed by six biological replicates with heat treatment at 98 °C. Last two columns reported the results of spiking the same amount of copies in water with and without heating treatment.

was loaded onto the surface of the metal collector in droplets of 1 µL each. We first positioned two droplets symmetrically along the length of the metal collector, and then rotated the it by 72 degrees to repeat this action at a new location until all 10 droplets were loaded. During the loading, the airflow of the biosafety cabinet was turned off and droplets were distributed evenly across the surface of the probe. When loading was completed, the metal collector was left to dry in air for 5 minutes, at the end of which nearly all loaded material had evaporated. Since we used a new pipette tip for every 1 µL droplet, 0.5 µL of the 10 µL was lost because small amount of liquid adhered to the inside of pipette tips. We adjusted the genome copy numbers calculation to account for this fact.

After heating, each tube was immediately placed in ice to cool down. We took a 7.4 µL heated sample to set up a 20 µL RT-qPCR reaction.

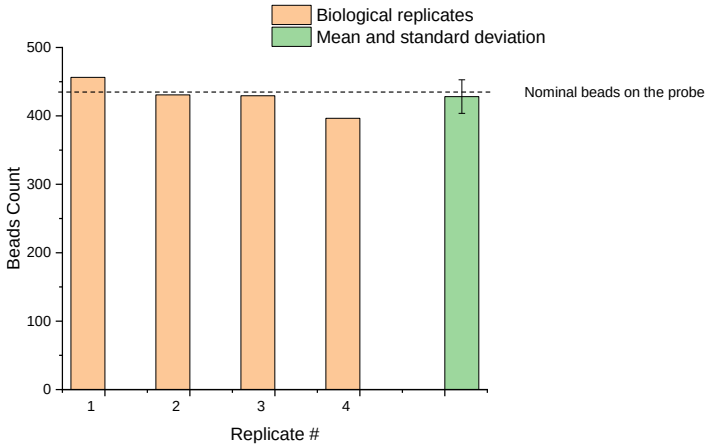

Figure S2: **FluoSpheres detachment test.** To demonstrate the consistency of our loading-extraction protocol, we loaded the metal collectors with the same number of FluoSpheres (430, as the lowest concentration of extraction test) and followed the steps outlined in Figure 3(a). The green bar on the right shows the mean and standard deviation over four biological replicates: 428 ± 24.

Enrichment

Calculations of the total mass of RNA in the enrichment device were conducted as follows. The molecular weight of single-stranded RNA was calculated with the following formula: MW = (# nucleotides $\times 320.5 +$

	No heat (on probe)	98 °C, (on probe)						No heat (in water)	98 °C (inwater)
Biological replicate #	-	1	2	3	4	5	6	-	-
Technical replicate #1	31.47	26.65	27.08	26.13	29.27	29.13	27.68	24.89	25.20
Technical replicate #2	31.72	26.63	27.00	26.22	28.92	29.13	27.05	24.48	24.78
Technical replicate #3	31.18	26.63	26.65	25.96	28.88	29.10	27.02	24.50	24.76
Technical replicate #4	30.99	26.48	26.63	25.84	28.90	28.91	26.92	24.35	24.75
Mean	31.34	26.60	26.84	26.04	28.99	29.07	27.17	24.56	24.87
Standard deviation	0.32	0.08	0.23	0.17	0.19	0.11	0.35	0.23	0.22
Diluted concentration (cp/µL)	2.81	68.01	57.79	99.07	13.61	12.94	46.38	268.14	216.65
Initial concentration (cp/µL)	7.60	183.81	156.19	267.75	36.79	34.99	125.35	724.71	585.53
Efficiency (%)	0.73	17.63	15.19	25.80	3.56	3.34	12.19	72.47	58.55

Table S2: **Results of of heat-extraction tests (220000 copies).** For each biological/technical replicate, the Ct value was reported. The first column was loading the same number of copies on the probe but with no heating treatment, followed by six biological replicates with heat treatment at 98 °C. Last two columns reported the results of spiking the same amount of copies in water with and without heating treatment.

159.0). Because the exact length of the quantitative synthetic SARS-CoV-2 RNA from ATCC is proprietary, we estimated the maximum possible length as 22.4 kb per copy using the information that the synthetic RNA is composed of fragments of the ORF1ab, E, and N genes [58]. This corresponds to an approximate molecular weight of at most 7 179 359 g / mol. For 300 genome copies in 250 µL of enrichment buffer (2 attomolar), the total mass is estimated to be: $7179359 \times 300/N_A \approx 3.6$ femtograms, where N_A is Avogadro's constant. Due to the assumptions used, this represents an upper bound on the mass of RNA in the device.

Images and diagrams of the electrophoresis bath and enrichment of stained DNA are displayed in Figure S3.

Fabrication of enrichment devices

Enrichment devices were fabricated by casting PDMS (Sylgard 184, Fisher Scientific, NC9285739) in custom-designed molds. The molds were created using a two-step process. First, the body of each mold was designed in SolidWorks and 3D-printed using a Formlabs stereolithography printer with clear resin (purchased through Protolabs). The geometry of the mold consisted of a semicircular sink with two 2.38 mm diameter holes bored through the flat ends (Figure 4a). After printing, molds were washed with 100 % isopropanol and cured in a UV oven for 30 minutes. Next, 7.5 cm stainless steel rods of 2.38 mm diameter were lightly greased with commercial petroleum jelly and inserted through the holes in each mold to form the channel running axially through the device (Figure 4a). Plastic spacers were used to create a press fit between the rod and the holes in the 3D printed part. The PDMS elastomer was prepared according to the manufacturer's instructions, mixed by vortexing, then cast in the molds. The PDMS-containing molds were degassed for 10 minutes and baked in a 65 °C oven for 2 hours. Excess petroleum jelly was removed from the channel walls using a clean room swab. The rod was extracted and the PDMS cast was removed using forceps. The first PDMS cast created in each mold was discarded.

After creation of the PDMS devices shown in Figure 4a, semipermeable membranes were attached to either end of the channel using PDMS as an adhesive. Briefly, double-layer cellulose 12-14 kDa molecular weight cutoff dialysis membranes (Spectrum Labs, 132678T) were cut into circles of 5 mm diameter using a biopsy punch (World Precision Instruments, 504532). Degassed uncured PDMS was applied to the flat end of the PDMS cast making a circle around each hole using a syringe with a blunt-end needle as an applicator. The applied PDMS was smoothed to a uniform thickness using a micropipette tip. Using forceps, the double-layer semipermeable membrane cutouts were centered on each hole and gently applied to the PDMS to create a seal. The PDMS sealant was allowed to cure in a 65 °C oven for 60 minutes. Then, a second ring of PDMS was applied to the outer portion of each membrane to improve the quality of the seal. The PDMS was cured at 65 °C for an additional 60 minutes.

Visualization of nucleic acid enrichment in enrichment devices

HCT 116 human colorectal cancer cells (ATCC, CCL-247) were cultured in DMEM (Gibco, 11965084) with 10% fetal bovine serum (Sigma Aldrich, F2442) and 1% penicillin-streptomycin (Life Technologies, 15140122).

Total RNA was isolated from these cells using a PureLink RNA Mini Kit (Invitrogen, 12183018A). 1 µg of RNA was diluted in 250 µL of LA to fill each enrichment device. SYBR Green II (Invitrogen, S7564), an RNA-specific nucleic acid stain, was prepared at 1x in the RNA-containing buffer and mixed prior to loading. Devices were imaged on a 470 nm LED transilluminator (IO Rodeo, IMG-04-02) before and after conducting enrichment at 300 V for 10 minutes using identical zoom, illumination, and exposure settings.

To visualize DNA enrichment, SYBR Safe™ Stain was prepared at 1x in LA with 1 µg DNA (Thermo Scientific, GeneRuler 1kb DNA Ladder, SM0312) and imaged every 6 minutes for 30 minutes in the running conditions described above. The device was also loaded with TriTrack three-color DNA loading dye (Thermo Scientific, R1161) alone and imaged after 15 minutes to confirm enrichment visually.

Simulation of nucleic acid enrichment in enrichment devices

The fluid dynamics simulation was performed using COMSOL Multiphysics. An axisymmetric geometry was used with matching dimensions as specified in Figure 4(b). At the ends of the channel, we applied a voltage of 300 V and water was assumed to be able to flow through the channel opening at a small but constant averaged velocity of 0.01 µm/ sec to emulate the semi-permeable membranes at two ends. We first simulated the steady flow generated by electroosmosis, and the ζ-potential of the PDMS channel was determined to be $\zeta_{\text{PDMS}} = -5 \sim -60\text{mV}$ [59, 60]. The diffusion coefficient of SARS-CoV-2 RNA can be estimated from the molecular dynamics simulations of single-stranded RNA, and it was determined to be $0.68 \sim 1.13 \times 10^{-12}\text{m}^2/\text{s}$ [61, 62, 63]. And the effective charge was estimated to be $-64 \sim -434$ for a 30kb genome [64]. These electrokinetic constants were varied within the above ranges to minimize the difference in outcomes between simulation and experiments. We chose $\zeta_{\text{PDMS}} = -13\,\text{mV}$, the effective charge $q_{\text{RNA}} = -120$ and a diffusion coefficient of $D_{\text{RNA}} = 1.13 \times 10^{-12}\text{m}^2/\text{s}$.

RT-qPCR

N2 forward (IDT, 10006824, 5'-TTACAAACATTGGCCGCAAA-3') and N2 reverse (IDT, 10006825, 5'-GCGCGACATTCCGAAGAA-3') primers were utilized in all reactions. The RT-qPCR reactions were prepared inside of a PCR-dedicated laminar flow hood or a BL2 biosafety hood, which were sterilized with UV light for 30 minutes. All lab work was conducted while wearing a N-95 mask, and materials and reagents were opened only inside of the hood. A clean-to-dirty workflow was followed, where we first prepared the RT-qPCR reactions by mixing the Luna Universal One-Step Reaction Mix, Luna WarmStart RT Enzyme Mix, and primers, while keeping the SARS-CoV-2 RNA sealed and outside of the hood. We then brought the SARS-CoV-2 RNA into the hood and mixed the RNA with the rest of the reagents to prepare the final RT-qPCR reactions. For each RT-qPCR reaction, the SARS-CoV-2 sample was suspended in a total volume of 7.4 µL in either nuclease-free water or LA buffer (5 mM). Subsequently, the 7.4 µL sample of SARS-CoV-2 was added to make a final volume of 20 µL according to Table S4 (1.85 mM final concentration of LA). The timing and temperatures utilized are shown on Table S5. To verify that the reagents, materials, and preparation area remained uncontaminated in each experiment, 12 NTC wells were prepared on every RT-qPCR plate used in the study and verified to be negative after 45 cycles (Figure S4 and S5).

Integration

As shown in Figure 5, we started with a series of 10-fold dilutions of ATCC-VP and aliquoted 10 µL at the end containing a defined number of copies of ATCC-VP. Before loading the ATCC-VP onto the metal collector, all working surfaces and equipment were wiped with RNaseZap™ Solution, and the ventilation of the biosafety cabinet was turned off to minimize evaporation during loading. A clean metal collector was picked from the sealed container using tweezers and placed upright on a magnet. A 2.5 µL pipette was used to transfer 1 µL out of the aliquoted 10 µL solution onto the surface of the metal probe (see "Heat Extraction" in Supplementary Materials for how droplets were loaded onto the probe). After loading, the metal probe was left to dry in the biosafety cabinet for 5 minutes as before (ventilation off). After loading, the probe was collected in a 2 mL microcentrifuge tube with 220 µL of nuclease-free water. The tube and metal probe were heated in the bath at 98 °C for 5 minutes before being transferred to ice to cool down as before. The tube was then brought back to the biosafety cabinet and the metal collector was removed with a magnet. We then measured the volume of the liquid left in the 2 mL tube. The number was later used to calculate how much additional buffer was needed to fill the enrichment device channel. The rest of the solution was

	5 minutes							
							Mean	Standard deviation
Ct (before)	33.7	33.73	34.8					
Concentration (copies/uL)	0.5478	0.5370	0.2646				0.43	
Ct (after)	31.48	32.3	32.01					
Concentration (copies/uL)	2.3784	1.3828	1.6751				1.77	
Fold change	5.57	3.24	3.92				4.14	1.20
Efficiency	0.16	0.09	0.11				0.12	0.04
	10 minutes							
							Mean	Standard deviation
Ct (before)	33.82	34.57	34.26	34.13	34.5	34		
Concentration (copies/uL)	0.5060	0.3081	0.3782	0.4122	0.3227	0.4492	0.39	
Ct (after)	31.73	31.8	32.07					
Concentration (copies/uL)	2.0159	1.9247	1.6100				1.84	
Fold change	5.17	4.93	4.13				4.72	0.55
Efficiency	0.15	0.15	0.12				0.14	0.02
	15 minutes							
							Mean	Standard deviation
Ct (before)	33.04	33.48	33.92	33.95	33.06	33.72		
Concentration (copies/uL)	0.8476	0.6336	0.4736	0.4643	0.8365	0.5406	0.61	
Ct (after)	31.51	31.45	31.16					
Concentration (copies/uL)	2.3317	2.4261	2.9390				2.55	
Fold change	3.80	3.95	4.79				4.16	0.53
Efficiency	0.11	0.12	0.14				0.12	0.02

Table S3: **Experimental results of enrichment at 5, 10 and 15 minutes and calculations of concentration fold changes and enrichment efficiencies.** For each time condition, we reported the Ct values of the samples from RT-qPCR before and after enrichment. Using the standard curve in Figure 4(e), we calculated the concentrations of SARS-CoV-2 RNA in the RT-qPCR reactions before and after enrichment and the fold changes in concentrations. The efficiencies were calculated following the definition in Figure 4(g).

Component	20 µL reaction	Final concentration
Luna Universal One-Step Reaction Mix (2X)	10 µL	1X
Luna WarmStart RT Enzyme Mix (20X)	1 µL	1X
N2 Forward Primer (10 µM)	0.8 µL	0.4 µM
N2 Reverse Primer (10 µM)	0.8 µL	0.4 µM
SARS-CoV-2 RNA in water or LA buffer	7.4 µL	variable

Table S4: **RT-qPCR reaction composition for SARS-CoV-2 detection in nuclease-free water or LA buffer**

Step	Temperature	Time	Cycles
Reverse Transcription	55°C	10 minutes	1
Initial Denaturation	95°C	1 minutes	1
Denaturation Extension	95°C 60°C	10 seconds 30 seconds	45
Melt curve	60-95°C	various	1

Table S5: **RT-qPCR timing and temperatures.**

supplemented with the appropriate volume of PCR-grade LA buffer stock (20x) and nuclease-free water to make a total input volume of 250 µL to the enrichment process (Figure S6). For enrichment, we followed the same protocol described in Section 2.3, running three devices at a time. At the end of enrichment, exactly 7.4 µL of sample was recovered near the anode of each device with a 10 µL pipette as before, followed by addition of RT-qPCR reagents to make a 20 µL reaction volume.

As mentioned in Section 2.4 of main text, we experimented with two different numbers of starting genome copies on the metal probe (430 and 500). The first number 430 corresponds to the # B we collected at the lowest concentration in Figure 2(d). From the master stock of ATCC-VP, we performed a series of 10-fold dilutions and made a 10 µL solution containing 430 copies of ATCC-VP. Then we used a 2.5 µL pipette to transfer 1 µL of this solution onto the surface of the metal probe. Due to the loss of liquid (residuals on the inner surface of pipette tips), 9.5 µL was actually loaded. In addition, at the end of heating heat-extraction, usually around 210 µL of liquid could be recovered. We aliquoted another 7.4 µL for RT-qPCR analysis as a control for no-enrichment, and some target molecules were also lost in this process. Eventually, the number of genome copies should be back-calculated as: $430 \times \frac{9.5\,\mu L}{10\,\mu L} \times \frac{(210-7.4)\mu L}{210\,\mu L} \approx 394$. The aliquoting step was also illustrated in the Figure S6. For the 500 genome copies, we did not have any loss due to the pipetting or aliquoting, so corrections were not made for this case.

We also conducted the integration tests for non-template controls (NTCs), and the results were displayed in Table S6.

NTC #	Ct value	NTC #	Ct value
1	ND	9	ND
2	ND	10	ND
3	ND	11	ND
4	ND	12	ND
5	ND	13	ND
6	ND	14	ND
7	ND	15	ND
8	ND		
Total detection rate:		0/15 (0%)	

NTC #	Ct value	NTC #	Ct value
1	ND	9	ND
2	ND	10	ND
3	ND	11	ND
4	ND	12	ND
5	ND	13	ND
6	ND	14	ND
7	ND	15	ND
8	ND		
Total detection rate:		0/15 (0%)	

Table S6: **Non-template controls in integration tests.** Left: these samples were collected from the 7.4 µL aliquots before enrichment (left side of Figure S6). Right: these samples were collected after enrichment (right side of Figure S6). All NTCs were negative.

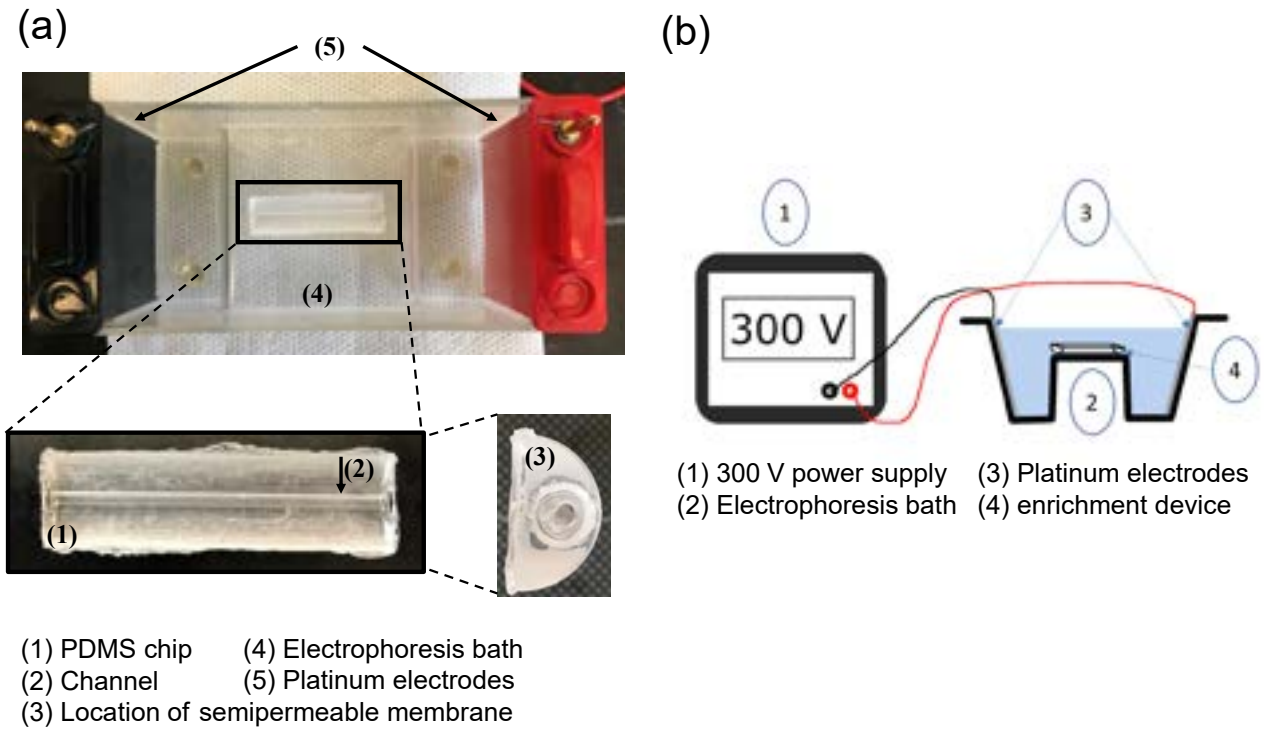

Figure S3: **Nucleic acid enrichment by electrophoresis.** (a) Photographs of the enrichment device and the electrophoresis bath used, in which the key elements are highlighted. (b) Schematic of the key elements of the enrichment process and their connections. (c) Enrichment of DNA 1 kb ladder stained with SYBR Safe dye. (d) Enrichment of TriTrack dye alone.

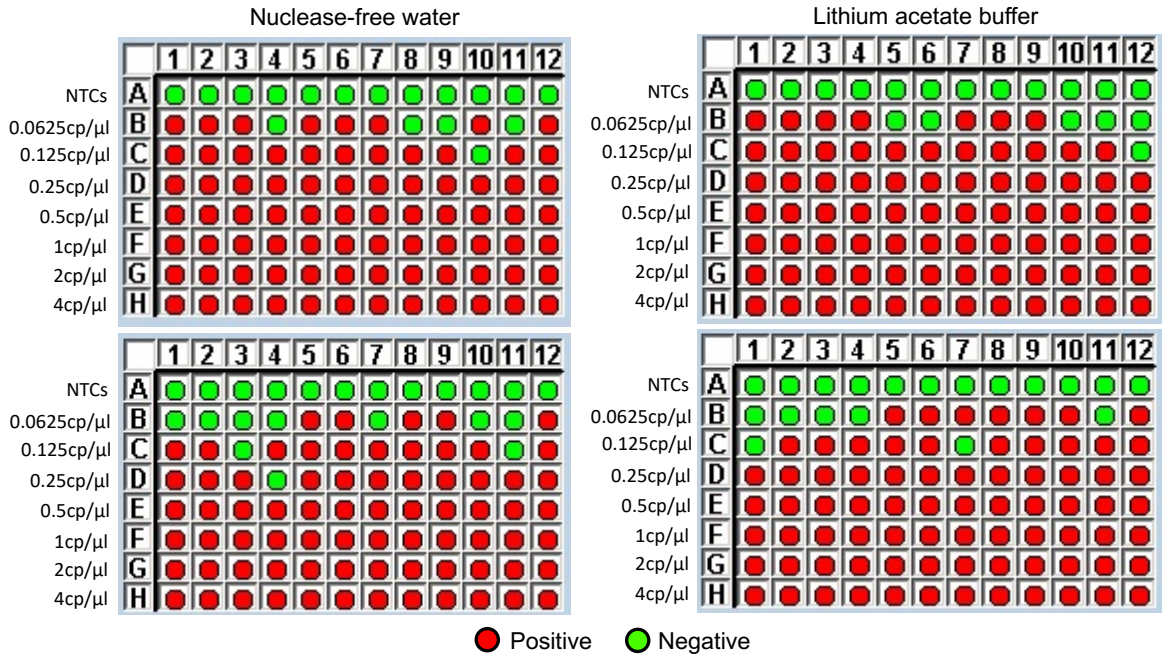

Figure S4: **Results of RT-qPCRs utilized to generate the standard curves for nuclease-free water and lithium acetate in LightCycler 480 Software.**

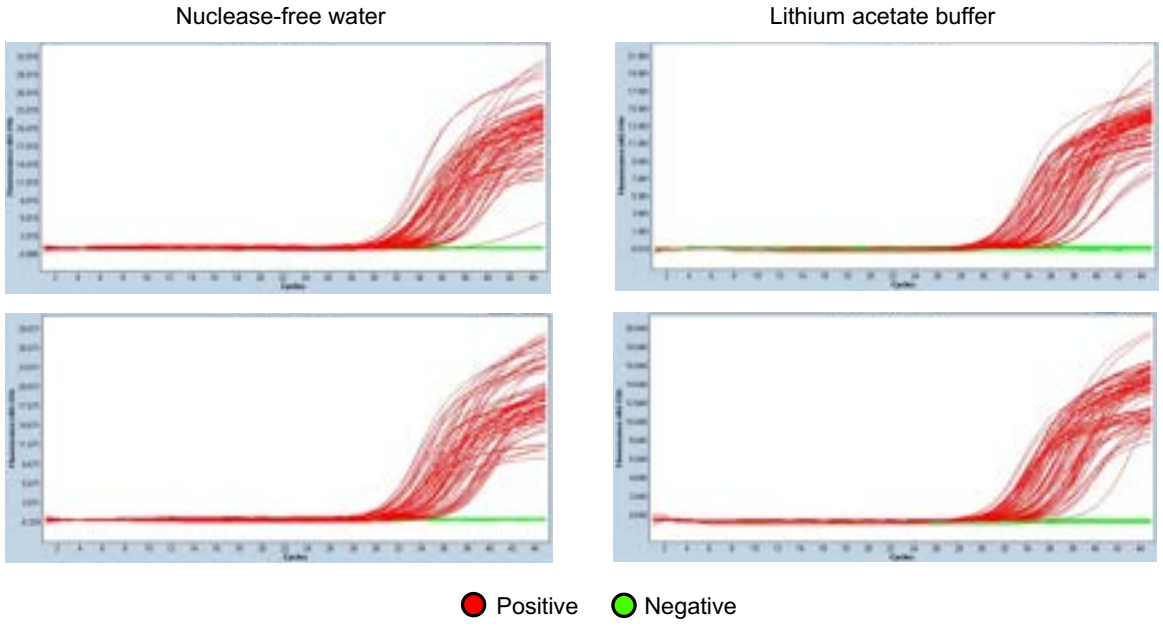

Figure S5: **Amplification curves of RT-qPCRs utilized to generate the standard curves for nuclease-free water and lithium acetate in LightCycler 480 Software.**

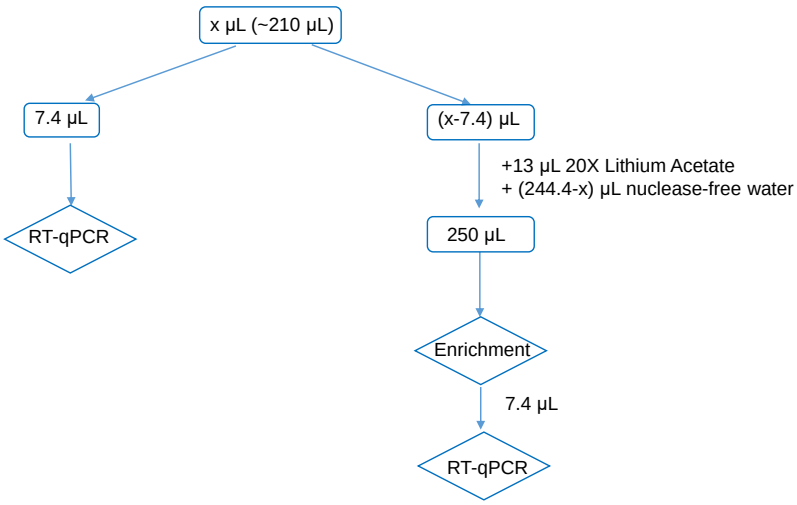

Figure S6: **Flow chart of the integration experiments with the 430 genome copies (NTCs as well)**